Computational Materials Science 194 (2021) 110435

Contents lists available at ScienceDirect

Computational Materials Science

journal homepage: www.elsevier.com/locate/commatsci

Editor's Choice

Elastic dipole tensors and relaxation volumes of point defects in concentrated random magnetic Fe-Cr alloys

Jan S. Wróbel [a,*], Marcin R. Zemła [a], Duc Nguyen-Manh [b], Pär Olsson [c], Luca Messina [d], Christophe Domain [e], Tomasz Wejrzanowski [a], Sergei L. Dudarev [b]

[a] Faculty of Materials Science and Engineering, Warsaw University of Technology, ul. Wołoska 141, 02-507 Warsaw, Poland
[b] UK Atomic Energy Authority, Culham Centre for Fusion Energy, Abingdon, Oxfordshire OX14 3DB, United Kingdom
[c] KTH Royal Institute of Technology, Department of Physics, 106 91 Stockholm, Sweden
[d] CEA, DES, IRESNE, DEC, F-13108 Cadarache Saint-Paul-Lez-Durance, France
[e] EdF-R&D, Département Matériaux et Mécanique des Composants, Les Renardières, F-77250 Moret sur Loing, France

ARTICLE INFO

Keywords:
Point defects
Fe-Cr alloys
Elastic dipole tensor
Density functional theory
Random magnetic systems
Relaxation volumes

ABSTRACT

Point defects in body-centred cubic Fe, Cr and concentrated random magnetic Fe-Cr are investigated using density functional theory and theory of elasticity. The volume of a substitutional Cr atom in ferromagnetic bcc Fe is approximately 18% larger than the volume of a host Fe atom, whereas the volume of a substitutional Fe atom in antiferromagnetic bcc Cr is 5% smaller than the volume of a host Cr atom. In an alloy, elastic dipole $\boldsymbol{P}$ and relaxation volume $\boldsymbol{\Omega}$ tensors of vacancies and self-interstitial atom (SIA) defects exhibit large fluctuations, with vacancies having negative and SIA large positive relaxation volumes. Dipole tensors of vacancies are nearly isotropic across the entire alloy composition range, with diagonal elements P_{ii} decreasing as a function of Cr content. Fe-Fe and Fe-Cr SIA dumbbells are more anisotropic than Cr-Cr dumbbells. We find that fluctuations of elastic dipole tensors of SIA defects are primarily associated with the variable crystallographic orientations of the dumbbells. Statistical properties of tensors $\boldsymbol{P}$ and Ω are analysed using their principal invariants, suggesting that point defects differ significantly in alloys containing below and above 10% at. Cr. The von Mises stresses caused by dumbbells are notably larger than those caused by vacancies. The relaxation volume of a vacancy depends sensitively on whether it occupies a Fe or a Cr lattice site. A correlation between elastic relaxation volumes and magnetic moments of defects found in this study suggests that magnetism is a significant factor influencing elastic fields of defects in Fe-Cr alloys.

1. Introduction

Defects are the stable strong local distortions of regular atomic order that form in crystalline metals and alloys under irradiation or during mechanical deformation [1]. Defects not only affect how a material responds to applied stress and deformation, but they also change electronic properties, including thermal and electrical conductivity, and magnetism.

Microstructural evolution of an alloy occurring as a result of accumulation of defects is driven by short- and long-range interactions of alloying elements with dislocations, surfaces, grain boundaries, and point defects. Short-range interactions, involving variation of chemical compositions in the vicinity of defects, can be investigated using Density Functional Theory (DFT) [2–7]. Long-range interaction between the defects is elastic, and it is mediated by the distortions that defects generate in the crystal lattice [8–17].

The fundamental quantities that determine the elastic fields and long-range elastic interaction between defects, are the elastic dipole and relaxation volume tensors [9–18]. These quantities can be computed using DFT or other atomic level simulations, and can then be used in the context of larger scale models, for example where the defects and ensembles of defects are treated as objects of continuum elasticity [19,20]. So far, elastic dipole and relaxation volume tensors of point defects have been investigated primarily for pure metals [9–18,21].

In Refs. [14,15] it was shown that the elastic field of an isotropic point defect in a cubic crystal, for example a vacancy, is fully defined by a single parameter, the elastic relaxation volume of the defect. On the other hand, a self-interstitial atom (SIA) defect often adopts an

* Corresponding author.
E-mail address: jan.wrobel@pw.edu.pl (J.S. Wróbel).

https://doi.org/10.1016/j.commatsci.2021.110435
Received 20 August 2020; Received in revised form 5 March 2021; Accepted 9 March 2021
Available online 5 April 2021

anisotropic configuration, and the treatment of its elastic field requires using several independent parameters defining the relaxation volume of the defect and its spatial orientation [14,15].

A vacancy, because of the isotropic nature of its dipole tensor, does not interact with a shear strain field even in an elastically anisotropic cubic material, whereas the anisotropic structure of an SIA defect enables elastic interaction with shear strain, applied externally or generated by other defects or dislocations [11]. The investigation of elastic dipole tensors and relaxation volumes, as well as other properties of point defect in concentrated alloys, is a challenging task since these quantities depend on the composition of the alloy, atomic short-range order as well as on the local environment of a defect [22–24]. In a magnetic alloy the structure of a defect is also affected by non-linear magneto-volume effects.

Here, we focus on the investigation of point defects in concentrated Fe-Cr alloys, which are the base alloy system underpinning the composition of many industrial steels. The phase stability and properties of magnetic Fe-Cr alloys were extensively explored theoretically [2–4,25–35] and experimentally [36–39]. The analysis performed in Ref. [40] showed that vacancies attract Cr atoms and hence may form vacancy-Cr clusters in dilute bcc Fe-Cr alloys. Investigation of point defects in dilute Fe-Cr alloys [26,29,31,34,41,42] shows that the formation energy of SIA dumbbells depends on the local configuration of Cr atoms surrounding a defect. However, to the best of authors' knowledge, elastic dipole and relaxation volume tensors of point defects, and the long-range elastic fields of such defects in concentrated Fe-Cr alloys have never been systematically explored.

In this paper, we study point defects in concentrated random Fe-Cr alloys, with Cr concentration up to 35%. Since estimating the relaxation volume of a defect using the stress method, which is described below, requires information about elastic constants of the material, which vary with alloy composition, elastic properties of random Fe-Cr alloys are investigated as a function of Cr content. To find the most stable point defect configurations, formation energies of defects were determined using concentration-dependent chemical potentials of Fe and Cr. Relaxation volumes of dumbbells are also correlated with the magnetic moments of atoms forming these defects. We also assess the difference between relaxation volumes of point defects computed using the stress method and full cell relaxation method [43,44].

2. Methodology

2.1. Elastic dipole tensors and relaxation volumes

A point defect induces a long range elastic field in the surrounding lattice. The energy of interaction between a localised defect and external homogeneous strain field $\epsilon_{ij}^{\text{ext}}$, arising from the quadratic cross-terms in the volume integral of the density of elastic energy of the defect and external field, is [8]

$$E = -P_{ij}\epsilon_{ij}^{\text{ext}}, \tag{1}$$

where repeated indices imply summation, and P_{ij} is the ij-th element of the elastic dipole tensor, $\boldsymbol{P}$, of the defect. This second-rank tensor is a fundamental quantity relating the elastic field of a defect and its atomic structure. Tensor $\boldsymbol{P}$ fully characterizes the elastic properties of a localised defect.

Elements of the dipole tensor of a defect can be computed using the equation [11,14,15,20,21,45]

$$P_{ij} = -V_{\text{cell}}\overline{\sigma}_{ij}, \tag{2}$$

where V_{cell} is the volume of the simulation cell and $\overline{\sigma}_{ij}$ is the difference between the average, macroscopic, stress in the cell containing the defect and in the pristine structure. It should be noted that, using the above definition of P_{ij}, the homogeneous stress experienced by the cell, which is built with the fixed lattice parameter, is not taken into account and thus the elastic dipole tensor of a defect is only related to the average stress required to comply with the fixed periodic boundary conditions.

In practice, the elements of an elastic dipole tensor are determined using either the above stress method, Eq. (2), where the average *strain* in the simulation cell is zero [14], and hence the cell volume and its shape remain fixed and only the positions of ions are relaxed. Alternatively, P_{ij} can be computed using the full cell relaxation method, where the cell volume and its shape are relaxed to the zero macroscopic stress condition [21,44]. The main difference between the two methods is that the latter one takes into account not only the elastic relaxation effects but also non-elastic non-linear relaxation occurring in the core of the defect as well as everywhere in the simulation cell [46]. The stress and cell relaxation methods are reviewed together with other possible methods for computing elastic dipole tensors in Refs. [13,21,44,45].

In the full cell relaxation method, the dipole tensor is computed from the elements of macroscopic strain associated with the relaxation of the cell to the zero stress condition

$$P_{ij} = V_{\text{cell}}C_{ijkl}\epsilon_{kl}^{\text{app}}, \tag{3}$$

where C_{ijkl} is the fourth-rank tensor of elastic stiffness and $\epsilon_{kl}^{\text{app}}$ is the macroscopic strain developing as a result of full relaxation of atomic positions and the shape of the simulation cell.

The dipole tensor is related to another fundamental tensor entity, also characterising the defect, *via* the following relation

$$P_{ij} = C_{ijkl}\Omega_{kl}, \tag{4}$$

where Ω_{kl} is the kl-th element of the so-called relaxation volume tensor, Ω. It is related to the elastic dipole tensor through the tensor of elastic compliance, S_{ijkl}:

$$\Omega_{ij} = S_{ijkl}P_{kl}. \tag{5}$$

Tensors S_{ijkl} and C_{ijkl} are related as [1]

$$C_{ijmn}S_{nmkl} = \frac{1}{2}\left(\delta_{ik}\delta_{jl} + \delta_{il}\delta_{jk}\right).$$

The energy of interaction between a defect and external elastic field can be expressed in terms of either the elastic dipole or relaxation volume tensor as [16]

$$E = -\Omega_{ij}\sigma_{ij}^{\text{ext}}, \tag{6}$$

where $\sigma_{ij}^{\text{ext}} = C_{ijkl}\epsilon_{kl}^{\text{ext}}$ is the stress tensor associated with external strain.

The elastic relaxation volume of a defect Ω_{rel} can be computed by taking the trace of the relaxation volume tensor

$$\Omega_{rel} = \text{Tr}\boldsymbol{\Omega} = \Omega_{11} + \Omega_{22} + \Omega_{33}. \tag{7}$$

Ω_{rel} is a convenient parameter characterizing the degree of the overall macroscopic expansion or contraction of the material due to the presence of defects in it [20]. Also, it describes the "size" interaction between the defects, whereas the deviatoric component of the relaxation volume tensor, *i.e.* its off-diagonal terms and differences between diagonal components, gives rise to the so-called "shape" interaction. In the limit where elastic relaxation around the defect is isotropic and the relaxation volume tensor of a defect is diagonal [20] $\Omega_{ij} = \frac{1}{3}\Omega_{rel}\delta_{ij}$, where δ_{ij} is the Kronecker delta-symbol, Eq. (6) can be further simplified as [47]

$$E = -\Omega_{ij}\sigma_{ij}^{\text{ext}} = -\frac{1}{3}\sigma_{ii}^{\text{ext}}\Omega_{rel} = p\Omega_{rel}, \tag{8}$$

where p is the hydrostatic pressure, $p = -\frac{1}{3}\sigma_{ii}^{\text{ext}}$.

To analyse elastic dipole and relaxation volume tensors of point defects, it is convenient to use the notion of principal invariants, which

are the quantities independent of the orientation of Cartesian coordinate axes. The formula relating a second-rank tensor ($\boldsymbol{A}$) and its principal invariants is [48]

$$\boldsymbol{A}^3 - I_1\boldsymbol{A}^2 + I_2\boldsymbol{A} - I_3\mathbb{1} = \overline{\overline{0}}, \tag{9}$$

where $\mathbb{1}$ is the identity tensor, $\overline{\overline{0}}$ is the zero matrix, and $I_1,\ I_2,\ I_3$ are the principal invariants that can be expressed as

$$I_1 = \mathrm{Tr}\boldsymbol{A}, \tag{10}$$

$$I_2 = \frac{1}{2}\left[(\mathrm{Tr}\boldsymbol{A})^2 - \mathrm{Tr}\left(\boldsymbol{A}^2\right)\right], \tag{11}$$

$$I_3 = \det\boldsymbol{A}. \tag{12}$$

The above relations apply to both elastic dipole and relaxation volume tensors ($\boldsymbol{A} = \boldsymbol{P}$ or $\boldsymbol{\Omega}$). In what follows, the invariants of an elastic dipole tensor will be denoted by $I_1^P,\ I_2^P$ and I_3^P, whereas those of the relaxation volume tensor by $I_1^\Omega,\ I_2^\Omega$ and I_3^Ω. It is worth noting that I_1^Ω is nothing but the relaxation volume of a defect, whereas the invariants of the elastic dipole tensor are directly related to the volume average von Mises stress σ_{vM} generated by the defects distributed periodically and homogeneously in the material. This stress can be evaluated from Eqs. (1), (2), (6), (10), (11) as [48]

$$\sigma_{vM} = \frac{1}{V_{cell}}\sqrt{\left(I_1^P\right)^2 - 3I_2^P}. \tag{13}$$

2.2. Elastic properties of alloys

Bulk elastic constants are required for finding the elements of elastic dipole tensor using full cell relaxation, see Eq. (3). Analysis performed in Ref. [44] shows that relaxation volumes of clusters of point defects (voids and interstitial loops) may vary significantly, depending on the interatomic potential. Hence, having a correct starting estimate for the elastic stiffness parameters of Fe-Cr alloys is important for the investigation of elastic dipole and relaxation volume tensors of defects in these alloys.

For pure elemental cubic crystals, the tensor of elastic constants C_{ijkl} can be parameterized using only three independent parameters, C_{11}, C_{12} and C_{44}, see [49]. Elastic properties of alloys are more complicated and generally there can be up to twenty-one non-zero independent elastic constants. Elastic constants of disordered alloys adopting crystal lattice with cubic symmetry can be approximated as

$$\overline{C}_{11} = \frac{C_{11} + C_{22} + C_{33}}{3}, \tag{14}$$

$$\overline{C}_{12} = \frac{C_{12} + C_{13} + C_{23}}{3}, \tag{15}$$

$$\overline{C}_{44} = \frac{C_{44} + C_{55} + C_{66}}{3}, \tag{16}$$

$$C_{14} = C_{15} = C_{16} = C_{24} = C_{25} = C_{26} = C_{34} = C_{35} = C_{36} = C_{45} = C_{46} = C_{56} = 0. \tag{17}$$

In this study, the second-order elastic constants were computed by deforming an unstrained equilibrium structure and analysing the corresponding variation of the total energy E_{tot} as a function of components of strain. Applied deformation changes the total energy as follows [49]

$$U = \frac{E_{tot} - E_0}{V_0} = \frac{1}{2}\sum_{i=1}^{6}\sum_{j=1}^{6} C_{ij}\epsilon_i\epsilon_j, \tag{18}$$

where E_0 is the total energy of the unstrained lattice, V_0 is the volume of an undistorted cell and C_{ij} are the elements of the elastic constant matrix in the Voigt notation. Indices i and j vary from 1 to 6 following the sequence xx, yy, zz, yz, xz, xy [49].

For each deformation, eight values of strain ($\pm0.2\%, \pm0.4\%, \pm0.6\%, \pm0.8\%$) were considered and the corresponding energies computed. Each curve showing how the total energy varies as a function of deformation was then fitted to a quadratic form and the respective elastic constants obtained. Since random Fe-Cr alloys are elastically anisotropic, we investigated the directional dependence of Young's modulus. The analysis are given in the Supplementary Information.

2.3. Formation energies of point defects

The formation energy of a vacancy or a self-interstitial atom (SIA) in an alloy is defined as

$$E_f^{vac,A} = E_{vac} - \left(E_{ref} - \mu_A\right) + E_{el}^{corr}, \tag{19}$$

$$E_f^{SIA,A} = E_{SIA} - \left(E_{ref} + \mu_A\right) + E_{el}^{corr}, \tag{20}$$

where E_{vac} and E_{SIA} are the total energies of structures containing a vacancy and a self-interstitial atom, respectively, and E_{ref} is the total energy of the corresponding reference structure containing no defect. μ_A is the chemical potential of atom A (here, a Cr or Fe atom), which was removed or inserted into the original structure in order to form a vacancy or a self-interstitial atom defect, respectively. E_{el}^{corr} is a correction term resulting from the conditions of vanishing average macroscopic strain (in the stress method) *and* periodicity [12–14,45]. Methods for evaluating E_{el}^{corr} are described in Refs. [12–14,16,21,45]. It should be noted that the origin of E_{el}^{corr} is purely elastic [45], and it does not include non-elastic effects [46]. Therefore, the formation energies of defects computed using full cell relaxation are usually lower than those computed using the stress method where the boundaries of the simulation cell are assumed fixed [12,45], even if the E_{el}^{corr} term is taken into account [44].

Chemical potentials of Fe and Cr atoms are estimated from the total energy of the system, where at $T = 0$ K and $p = 0$ Pa in the thermodynamic limit [50] $E = \mu_{Fe}N_{Fe} + \mu_{Cr}N_{Cr}$, where N_{Fe} and N_{Cr} are the numbers of Fe and Cr atoms in the corresponding structure, respectively. Using this expression, we find the difference between the minimum substitutional energies $\Delta E^{Fe\to Cr}$ and $\Delta E^{Cr\to Fe}$ [51] as

$$\mu_{Cr} - \mu_{Fe} = \frac{1}{2}\left(\Delta E^{Fe\to Cr} - \Delta E^{Cr\to Fe}\right). \tag{21}$$

For each composition of the alloy, the minimum substitution energies are evaluated from the total energy difference between the reference structure and three structures, for each element, where a randomly chosen Fe (or Cr) atom has been replaced by a Cr (or Fe) atom.

2.4. Computational details

All the total-energy calculations were performed using density functional theory in the plane-wave basis, and pseudopotentials derived within the projector augmented wave (PAW) method [52,53] implemented in the Vienna Ab inito Package (VASP) code [54,55]. The PAW pseudopotentials used here did not include the semicore electrons. Exchange and correlation effects were treated in the generalized gradient approximation with the Perdew-Burke-Ernzerhof [56] parametrization. Collinear spin-polarized calculations, with a Vosko-Wilk-Nusair spin interpolation of the correlation potential, were carried out assuming that the initial magnetic moments of Fe and Cr atoms were 3 and −1 Bohr magnetons (μ_B), respectively. The magnetic moments of Cr atoms were treated as being initially antiferromagnetically aligned with respect to the ferromagnetically ordered magnetic moments of Fe atoms. The structures contained 250 (±1 Fe/Cr) atoms in the form of $5 \times 5 \times 5$ supercells with conventional body-centred cubic structure. Non-

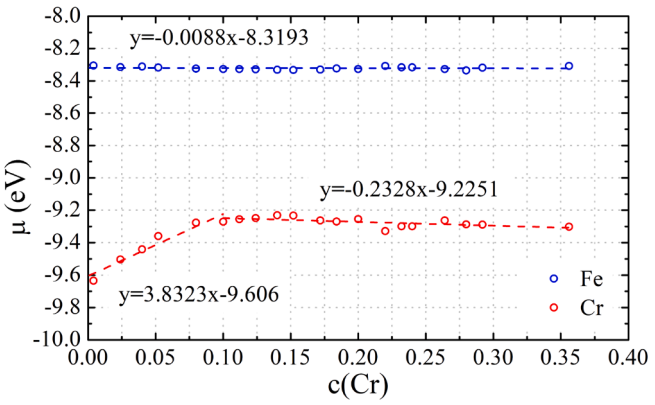

Fig. 1. Chemical potentials of Fe and Cr derived from DFT simulations involving full cell relaxation. Dashed blue and red lines show the interpolated values of μ_{Fe} and μ_{Cr} as functions of Cr content (see Table A.2).

collinear magnetic effects [57] were not treated in this study. The total energies were found using the Monkhorst-Pack [58] scheme to sample the Brillouin zone. A $3 \times 3 \times 3$ k-point grid was used when performing atomic relaxations. Structures of point defects in concentrated random Fe-Cr alloys, with concentrations up to 35% at. Cr, were taken from Ref. [59] where a DFT database of point-defect relaxation energies and migration barriers was used for training neural-network models. Since Cr atoms are distributed randomly in the alloy structures included in the database, this study describes properties of point defects in concentrated *random* Fe-Cr alloys where the effects associated with short-range order are not considered.

In this work, two types of DFT calculations were performed:

- *fixed volume calculations* – these were performed using the same parameters as in Ref. [59,60], namely the lattice parameter of 2.831 Å, the plane-wave energy cut-off of 300 eV and the convergence criteria of 10^{-3} eV/cell and 10^{-4} eV/cell set for the total energies of ions and electrons, respectively. The energies of structures containing defects and residual stresses given in Ref. [59] were directly comparable with results of calculations performed in this study, and they were used for determining the formation energies as well as elastic dipole and relaxation volume tensors of point defects using the stress method.
- *calculations involving full cell relaxation* – these were performed using the energy cut-off of 400 eV and convergence criteria of 10^{-3} eV/Å and 10^{-6} eV/cell set for the total energies of ions and electrons, respectively. These calculations were used for determining the chemical potentials and elastic properties of alloys, as well as calculating the formation energies and relaxation volumes of defects using the cell relaxation method. We remind the reader that at $T = 0$ K, an accurate evaluation of chemical potentials requires setting $p = 0$ Pa, which implies full relaxation of the simulation cell.

The impact of the choice of computational approach on the accuracy of results is discussed in Section 4.3 below.

3. Results

3.1. Chemical potentials and formation energies of defects

Chemical potentials of Fe (μ_{Fe}) and Cr (μ_{Cr}) atoms in random Fe-Cr alloys were estimated from DFT simulations assuming either a fixed volume of the simulation cell, or full atomic and volume relaxation. Simulations were performed for twenty alloy structures with concentrations chosen approximately evenly across the range of Cr concentrations. Fig. 1 shows that the chemical potential of Fe in Fe-Cr alloys remains almost constant over the entire range of compositions explored in this study, and its value is close to the chemical potential of pure bcc Fe, which is −8.31 eV. The chemical potential of Cr atoms behaves differently below and above approximately 10% at. Cr, which corresponds to the Cr solubility limit in Fe-Cr alloys at low temperature [61]. Below the solubility limit, μ_{Cr} increases as a function of Cr content, whereas above the solubility limit it slowly decreases as a function of Cr concentration. It should be noted that earlier theoretical and experimental studies show that properties of Fe-Cr alloys differ significantly below and above approximately 10% at. Cr [3,4,30,33,62]. Hence, not only the analysis of chemical potentials but also the study of formation energies, elastic dipole and relaxation volume tensors for point defects in Fe-Cr alloys in what follows is going to be split into two separate investigations, focusing on alloys with compositions below and above 10% at. Cr.

We note that the results shown in Fig. 1 are insensitive to the energy cut-off and the internal degrees of freedom, for example the chemical potentials derived from fixed-volume DFT simulations are virtually identical to those derived from simulations involving full cell relaxation – the difference is smaller than 0.1%. Bearing this in mind, still only the values obtained with full relaxation of simulation cells, corresponding to vanishing pressure $p = 0$ Pa, are shown in Fig. 1. Interpolated values of chemical potentials of Fe and Cr shown by dashed lines in Fig. 1 were used as a reference when evaluating the formation energies of point defects in Fe-Cr alloys. Values of μ_{Fe} for pure bcc Fe and μ_{Cr} for pure anti-ferromagnetic bcc Cr were derived from the total energies of bcc Fe and Cr, respectively. Values of μ_{Cr} in bcc Fe and μ_{Fe} in anti-ferromagnetic bcc Cr were computed using the method described in Section 2.4 for the structures containing one Cr atom in bcc Fe and one Fe atom in bcc Cr, respectively. The computed formation energies of defects in bcc Fe matrix and bcc anti-ferromagnetic Cr matrix are given in Table 1.

Since most of the results for Fe-Cr alloys were obtained using fixed volume simulations cell, defined by the lattice parameter of pure Fe $a = 2.831$ Å, all the results for Cr given in this study were also computed assuming this lattice parameter. The computed formation energies include the correction term resulting from the periodic boundary conditions and the requirement of vanishing average strain [14,45].

In agreement with earlier studies [18,63], the computed formation energies of vacancies are significantly smaller than those of SIAs defects. The formation energies of defects in bcc Cr are notably larger than in bcc Fe. In accord with Refs. [18,64], the most stable configuration of a SIA defect in pure Fe is a $\langle 110 \rangle$ dumbbell, with the energy of formation of $E_{form} = 4.019$ eV found in our calculations. This formation energy is more than 0.7 eV lower than the formation energy of a self-interstitial atom defect with a $\langle 111 \rangle$ orientation.

In agreement with Refs. [15,65], we find that the most stable configuration of a Cr-Cr dumbbell in pure anti-ferromagnetic bcc Cr is a symmetry-broken $\langle 11\xi \rangle$ dumbbell, where ξ is 0.345. The difference between E_{form} of $\langle 11\xi \rangle$ SIA and E_{form} of $\langle 110 \rangle$ and $\langle 111 \rangle$ SIAs in pure Cr is 0.14 eV and 0.23 eV, respectively. This shows that the difference between energies of various SIA dumbbell configurations in bcc Cr is smaller than those in bcc Fe.

A symmetry-broken $\langle 11\xi \rangle$ configuration is also the most stable one for a Cr-Cr dumbbell in Fe matrix. This agrees with results from Ref. [26] showing that a Cr-Cr $\langle 110 \rangle$ dumbbell configuration in the presence of additional Cr atom in the neighbourhood (lowering the symmetry of a structure) may transform into a lower energy configuration, for example a $\left\langle 22\bar{1} \right\rangle$ Cr-Cr dumbbell.

A mixed Fe-Cr $\langle 110 \rangle$ dumbbell is the most stable mixed SIA defect configuration in bcc Fe matrix. Fig. 3a and b show that it can be formed either by adding a Cr atom to a Fe site or by adding a Fe atom to a Cr site. The formation energies of a Fe-Cr $\langle 110 \rangle$ dumbbell in the former and latter cases are 3.964 eV and 3.975 eV, respectively. In both cases, formation energies of Fe-Cr dumbbells were more than 0.04 eV lower than that of a $\langle 110 \rangle$ Fe-Fe, in agreement with Ref. [66], and they were

Table 1
Formation energies of defects and elements of elastic dipole tensors P_{ij} (in eV) of defects, relaxation volume tensors Ω_{ij} (in Å^3), relaxation volumes of defects and substitutional atoms Ω_{rel} (in Å^3) and relaxation volumes Ω^{at}_{rel} expressed in the units of atomic volume $\Omega_0 = a^3/2$. The reference atomic volume $\Omega_0 = 11.345$ Å^3 corresponds to the bcc lattice parameter of $a = 2.831$ Å.

	E_{form}	P_{11}	P_{22}	P_{33}	P_{12}	P_{23}	P_{31}	$\frac{P_{11}}{P_{22}}$	Ω_{11}	Ω_{22}	Ω_{33}	Ω_{12}	Ω_{23}	Ω_{31}	Ω_{rel}	Ω^{at}_{rel}
								Fe								
$(\mathrm{Vac})_{Fe}$	2.183	−3.682	−3.682	−3.682	0.000	0.000	0.000	1.00	−1.015	−1.015	−1.015	0.000	0.000	0.000	−3.045	−0.268
Ref. [15]	2.190	−3.081	−3.081	−3.081	0.000	0.000	0.000	1.00	−0.831	−0.831	−0.831	0.000	0.000	0.000		−0.220
$(\mathrm{Cr})_{Fe}$		2.531	2.531	2.531	0.000	0.000	0.000	1.00	0.698	0.698	0.698	0.000	0.000	0.000	2.093	0.184
$(\mathrm{Fe\text{-}Fe})^{\langle 110\rangle}_{Fe}$	4.019	24.853	20.534	20.534	0.000	4.620	0.000	1.21	6.851	5.660	5.660	0.000	1.274	0.000	18.171	1.602
Ref. [15]	4.321	25.832	21.143	21.143	0.000	5.122	0.000	1.22	9.777	4.294	4.302	0.000	3.819	0.000		1.620
$(\mathrm{Fe\text{-}Fe})^{\langle 111\rangle}_{Fe}$	4.762	21.596	21.596	21.596	5.204	5.204	5.204	1.00	5.953	5.953	5.953	1.435	1.435	1.435	17.859	1.574
$(\mathrm{Fe\text{-}Cr})^{\langle 110\rangle}_{Fe}$	3.964	23.756	21.826	21.826	0.000	4.691	0.000	1.09	6.548	6.016	6.016	0.000	1.293	0.000	18.581	1.638
$(\mathrm{Fe\text{-}Cr})^{\langle 110\rangle}_{Cr}$	3.975	21.065	19.136	19.136	0.000	4.691	0.000	1.10	5.807	5.275	5.275	0.000	1.293	0.000	16.356	1.442
$(\mathrm{Cr\text{-}Cr})^{\langle 110\rangle}_{Cr}$	4.501	19.472	22.269	22.269	0.000	6.160	0.000	0.87	5.367	6.138	6.138	0.000	1.698	0.000	17.644	1.555
$(\mathrm{Cr\text{-}Cr})^{\langle 11\xi\rangle}_{Cr}$	4.465	20.693	21.048	21.048	1.576	5.045	1.576	0.98	5.704	5.802	5.802	0.434	1.391	0.434	17.307	1.526
$(\mathrm{Cr\text{-}Cr})^{\langle 111\rangle}_{Cr}$	4.554	20.092	20.092	20.092	4.585	4.585	4.585	1.00	5.538	5.538	5.538	1.264	1.264	1.264	16.614	1.462
$(\mathrm{Cr\text{-}Cr})^{\langle 110\rangle}_{Fe}$	4.481	22.145	24.960	24.960	0.000	6.160	0.000	0.89	6.104	6.880	6.880	0.000	1.698	0.000	19.864	1.751
$(\mathrm{Cr\text{-}Cr})^{\langle 11\xi\rangle}_{Fe}$	4.446	23.384	23.738	23.738	1.576	5.045	1.576	0.98	6.446	6.543	6.543	0.434	1.391	0.434	19.532	1.722
$(\mathrm{Cr\text{-}Cr})^{\langle 111\rangle}_{Fe}$	4.535	22.782	22.782	22.782	4.585	4.585	4.585	1.00	6.280	6.280	6.280	1.264	1.264	1.264	18.839	1.661
								Cr								
$(\mathrm{Vac})_{Cr}$	2.717	−7.753	−7.753	−7.753	0.000	0.000	0.000	1.00	−2.225	−2.225	−2.225	0.000	0.000	0.000	−6.675	−0.588
Ref. [15]	3.004	−5.777	−5.777	−5.777	0.000	0.000	0.000	1.00	−1.618	−1.618	−1.618	0.000	0.000	0.000		−0.414
$(\mathrm{Fe})_{Cr}$		−0.726	−0.726	−0.726	0.000	0.000	0.000	1.00	−0.208	−0.208	−0.208	0.000	0.000	0.000	−0.625	−0.055
$(\mathrm{Cr\text{-}Cr})^{\langle 110\rangle}_{Cr}$	6.262	16.410	21.083	21.083	0.000	4.886	0.000	0.78	4.709	6.050	6.050	0.000	1.402	0.000	16.809	1.482
Ref. [15]	6.515	18.955	20.530	20.530	0.000	4.790	0.000	0.92	5.166	5.820	5.820	0.000	3.757	0.000		1.434
$(\mathrm{Cr\text{-}Cr})^{\langle 11\xi\rangle}_{Cr}$	6.116	19.755	18.445	18.445	1.098	3.629	1.098	1.07	5.669	5.293	5.293	0.315	1.041	0.315	16.256	1.433
Ref. [15]	6.361	21.882	18.389	18.389	2.058	4.040	2.058	1.19	6.436	4.987	4.987	1.614	3.168	1.614		1.400
$(\mathrm{Cr\text{-}Cr})^{\langle 111\rangle}_{Cr}$	6.354	18.056	18.056	18.056	3.682	3.682	3.682	1.00	5.182	5.182	5.182	1.057	1.057	1.057	15.545	1.370
Ref. [15]	6.617	18.728	18.728	18.728	4.617	4.617	4.617	1.00	5.244	5.244	5.244	3.622	3.622	3.622		1.343
$(\mathrm{Fe\text{-}Cr})^{\langle 110\rangle}_{Cr}$	5.085	22.180	16.622	16.622	0.000	3.753	0.000	1.33	6.365	4.770	4.770	0.000	1.077	0.000	15.905	1.402
$(\mathrm{Fe\text{-}Cr})^{\langle 110\rangle}_{Fe}$	5.108	23.048	17.489	17.489	0.000	3.753	0.000	1.32	6.614	5.019	5.019	0.000	1.077	0.000	16.652	1.468
$(\mathrm{Fe\text{-}Fe})^{\langle 110\rangle}_{Fe}$	4.057	25.438	15.277	15.277	0.000	4.337	0.000	1.67	7.300	4.384	4.384	0.000	1.245	0.000	16.068	1.416

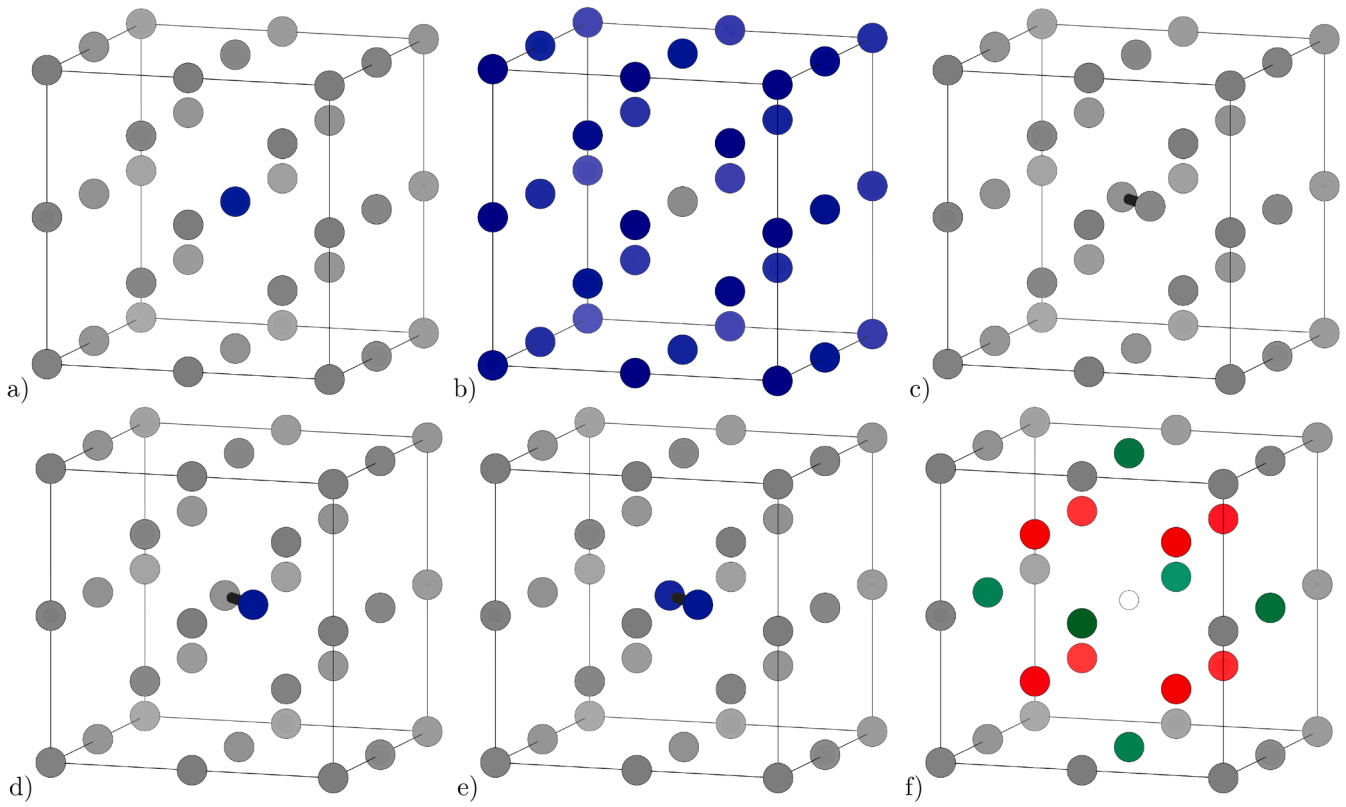

Fig. 2. Schematic representation of structures: (a) a Cr atom in bcc Fe, (b) a Fe atom in bcc Cr, (c) Fe-Fe, (d) Fe-Cr and (e) Cr-Cr ⟨110⟩ dumbbells in bcc Fe. Fe and Cr atoms are shown as grey and blue spheres, respectively. (f) Schematic representation of atoms in the neighbourhood of a defect (white sphere). Atoms in the first and second nearest neighbour shells are shown by red and green spheres, respectively.

0.48 eV lower than the formation energy of a ⟨11ξ⟩ Cr-Cr dumbbell.

In bcc Cr matrix, the difference between the energies of the most and least stable dumbbell configurations is significantly larger than in bcc Fe. The formation energy of a ⟨110⟩ Fe-Fe SIA in bcc Cr equals 4.057 eV, and it is more than 1 eV and 2 eV smaller than that of the most stable Fe-Cr and Cr-Cr dumbbells, respectively.

The formation energies of approximately 300 vacancy and 400 dumbbell configurations derived from fixed cell volume DFT simulations are shown, as functions of Cr content and the number of Cr atoms in the local environment of a defect, in Fig. 4a–d. The figures show that the formation energies of vacancies and SIA dumbbells fluctuate significantly, depending on the alloy composition and the local chemical environment of a defect.

To separate the role of the two effects and investigate properties of defects only as functions of the number of Cr atoms in their local environment, further 120 DFT calculations were performed for the defect-free structures of Fe-Cr alloys containing 5% at. Cr, and the same structures containing defects. Even for one alloy composition and the same number of Cr atoms in the 1st and 2nd nearest-neighbour (NN and NNN, see Fig. 2f) coordination shells around a defect, formation energies fluctuate by as much as 1 eV. This shows that the defect formation energies depend not only on parameters like the average alloy composition or the number of Cr atoms in the NN and NNN coordination shells, but also on the configuration of Cr atoms around a defect.

Vacancies in Fe-Cr alloys can be formed by removing either a Fe atom or a Cr atom from a lattice site, see Fig. 3c and d. Fig. 4a, c and e, show that there is a notable difference between the formation energies of vacancies on Fe and Cr sites. The average formation energy of a vacancy on a Fe site decreases slightly as a function of Cr content from approx. 2.1 eV at low Cr concentration to approx. 2.0 eV at 30% at. Cr. On the other hand, the average value of E_{form} for a vacancy on a Cr site increases with Cr content. The increase is more rapid in the range of Cr concentration below 10% at. Cr. Formation energies of vacancies on Cr sites are also more scattered than those associated with Fe sites, an effect that is probably related to the magnetic frustration of Cr atoms in bcc Fe matrix.

Fig. 4c shows the formation energy of a vacancy as a function of the number of Cr atoms N_{Cr}^{def} in the NN and NNN shells around a defect. The data span the entire range of alloy compositions considered here, with a separate Fig. 4e showing the data for Fe-5%Cr alloys. Since the variation of formation energies as a function of Cr concentration differs for configurations involving small and large values of N_{Cr}^{def}, the results are divided into two intervals where N_{Cr}^{def} is smaller or larger than 3. The value of 3 was chosen for two reasons. Firstly, according to our statistical analysis, it was the optimal value for which the fitting of trend lines was the best for vacancies and dumbbells simultaneously. Secondly, this choice enables a direct comparison of trend lines obtained for small values of N_{Cr}^{def} with the results computed for Fe-5%Cr alloys, where defects are surrounded by up to three Cr atoms in the NN and NNN shells.

The variation of the average formation energy of vacancies in Fe-5% Cr alloy is similar to the variation found for other Cr concentrations. For the smaller number of Cr atoms, Fig. 4c and e show that the formation energy E_{form} of a vacancy on either Fe and Cr sites decreases with increasing N_{Cr}^{def}. The rate of variation is more rapid for vacancies on Cr sites. For N_{Cr}^{def} larger than 3, the formation energy of a vacancy on a Fe site slightly decreases whereas that on a Cr site increases.

The variation formation energies of dumbbells as a function of Cr content is significantly different below and above approximately 10% at. Cr, see Fig. 4b for more detail. Above 10% at. Cr concentration, the average values of E_{form} of Fe-Cr and Cr-Cr SIAs remain almost constant, whereas below that concentration there is a rapid decrease of E_{form} as a function of Cr content. Only the slope of the trend line for E_{form}

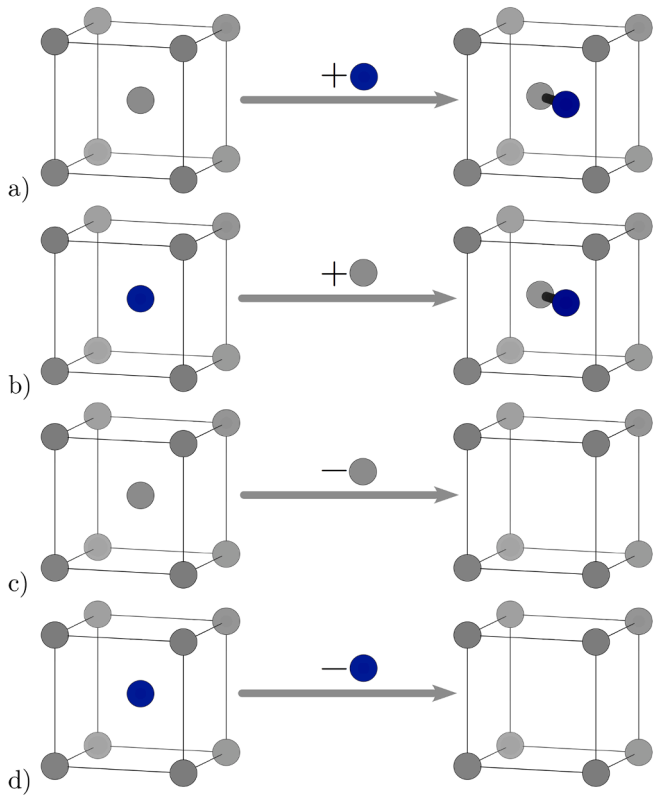

Fig. 3. Schematic representation of the process of formation of a mixed Fe-Cr dumbbell (a) by adding a Cr atom to a Fe site and (b) by adding a Fe atom to a Cr site. Schematic representation of formation of a vacancy (c) on a Fe site and (d) on a Cr site. Fe and Cr atoms are shown by grey and blue spheres, respectively.

computed for Fe-Fe SIAs remains similar over the whole considered range of Cr concentrations. Similarly to bcc Fe matrix, Fe-Cr dumbbells are generally the most stable interstitial defects in Fe-Cr alloys in the range of alloys compositions explored in this study. They exhibit the lowest mean values of E_{form} over the concentration range up to approximately 32% at. Cr. For each composition up to approximately 10–12% at. Cr, the most stable Fe-Cr SIA exhibits the lowest E_{form} among all the computed dumbbell configurations. For larger Cr concentrations, the Cr-Cr and Fe-Fe dumbbells may be more stable than the Fe-Cr SIAs.

Similarly to the variation of the formation energy of dumbbells as a function of Cr content, values of E_{form} shown in Fig. 4d vary differently for smaller and larger values of N_{Cr}^{def}. For Fe-Cr and Cr-Cr SIAs, the average value of E_{form} decreases and then slightly increases as a function of N_{Cr}^{def} when N_{Cr}^{def} is smaller and larger than 3, respectively. For Fe-Fe SIAs, the mean value of E_{form} decreases as a function of N_{Cr}^{def} over the range of N_{Cr}^{def}. For every value of N_{Cr}^{def}, Fe-Cr SIAs have the lowest mean E_{form}. However, for the majority of N_{Cr}^{def}, the most stable Cr-Cr dumbbells have smaller E_{form} than the most stable Fe-Cr and Fe-Fe SIAs.

Similarly to the case of vacancies, the trend lines of mean E_{form} for Fe-Fe and Fe-Cr dumbbells as a function of N_{Cr}^{def} in Fe-5%Cr alloy are generally similar to those found for other Cr concentrations, however the values are usually larger, as seen from the comparison of Fig. 4d and f. The largest difference is found for Cr-Cr dumbbells, for which the mean E_{form} in the Fe-5%Cr alloy does not decrease as a function of N_{Cr}^{def} as rapidly as for other Cr concentrations. As a result, the mean value of E_{form} for a structure with three Cr atoms in the local environment of a defect in the Fe-5%Cr alloy is approximately 0.5 eV larger than the one averaged over structures with the same N_{Cr}^{def} value in all the other Fe-Cr alloys. This may stem from the fact that the magnitudes of magnetic moments of Cr atoms vary significantly as a function of Cr composition in Fe-Cr alloys [3,25,33], and this may affect the value of E_{form} for Cr-Cr dumbbells. The strong dependence on Cr concentration of the formation energies of Cr-Cr interstitial defect may also explain the larger spread of their values in comparison with Fe-Fe and Fe-Cr dumbbell defects, see Fig. 4b and d.

Equations interpolating the variation of formation energies of vacancies and dumbbells as a function of Cr concentration and a number of Cr atoms in NN and NNN are given in Table A.2 in Appendix.

3.2. Elastic properties

To investigate elastic properties of disordered Fe-Cr alloys, and their variation as a function of Cr content, 21 random structures with Cr content up to 40% at. were fully relaxed by simultaneously minimizing atomic forces and components of the global stress tensor. Average lattice parameters of the structures are shown in Fig. 5a. The values found in our calculations are in agreement with earlier DFT results obtained using special quasi-random structures [67] and are smaller than the values obtained using the coherent potential approximation (CPA) [67,68]. We note that the experimental lattice parameters [69,70] are significantly higher than all the predicted values. This is likely associated with the approximations involved in the exchange-correlation functionals [67,68]. Also, calculations predict a visible maximum of the lattice parameter for alloys with Cr content between 7 and 12% at. Cr, which is less well pronounced in the experimental data.

Elastic properties of a disordered Fe-10%Cr alloy structure evaluated using various approximations are summarised in Table S1 in the Supplementary Materials. The difference between elastic properties calculated using different approaches does not exceed 1%. Therefore, it is appropriate to use the elastic constants of disordered Fe-Cr alloys derived from Eqs. (14)–(17). To verify how the elastic properties vary depending on the specific atomic configurations of random Fe-Cr structures, calculations were performed for three additional structures of Fe-5%Cr alloy. As Fig. 5 shows, the difference between the maximum and minimum values of each elastic constant does not exceed 3%. Since the differences between elastic properties of Fe-Cr alloys with different compositions can be an order of magnitude larger, the effect of atomic arrangement in random Fe-Cr structures can be safely neglected in the context of this study, in agreement with the principle that since the treatment of elastic properties of an alloy implies taking the macroscopic thermodynamic limit, the role of microscopic fluctuations of local atomic arrangements is expected to be small.

Average elastic constants $\overline{C}_{11}$, $\overline{C}_{12}$, $\overline{C}_{44}$ of random Fe-Cr structures plotted as functions of Cr concentration are shown in Fig. 5b–d. They were computed for 21 random structures with Cr content up to 40%. For each fully relaxed structure, nine elastic constants were computed and average elastic constants $\overline{C}_{11}$, $\overline{C}_{12}$, $\overline{C}_{44}$ were evaluated using Eqs. (14)–(17). Results for $\overline{C}_{11}$, $\overline{C}_{12}$, $\overline{C}_{44}$ were interpolated using analytical formula in order to then use them in the calculations of elastic interactions and relaxation volumes for each alloy composition, see Fig. 5b–d. Analysis of earlier theoretical studies shows that the computed elastic constants of Fe-Cr alloys can vary depending on method used and the chosen value of the lattice parameter. The difference between the calculated values can be as large as 30–40 GPa (see Fig. 5a and b). For pure Fe, theoretical predictions often overestimate the experimental values of C_{11} and usually C_{12}, and underestimate C_{44}.

In the calculations of relaxation volume tensors and relaxation volumes of point defects in bcc Fe and bcc Cr we used the following computed values of elastic constants: $C_{11} = 277.29$ GPa, $C_{12} = 151.29$ GPa and $C_{44} = 96.93$ for bcc Fe, and $C_{11} = 459.73$ GPa, $C_{12} = 49.29$ GPa and $C_{44} = 93.65$ for bcc Cr.

The investigation of polycrystalline elastic properties and directional dependence of the Young's modulus of Fe-Cr alloys, together with the

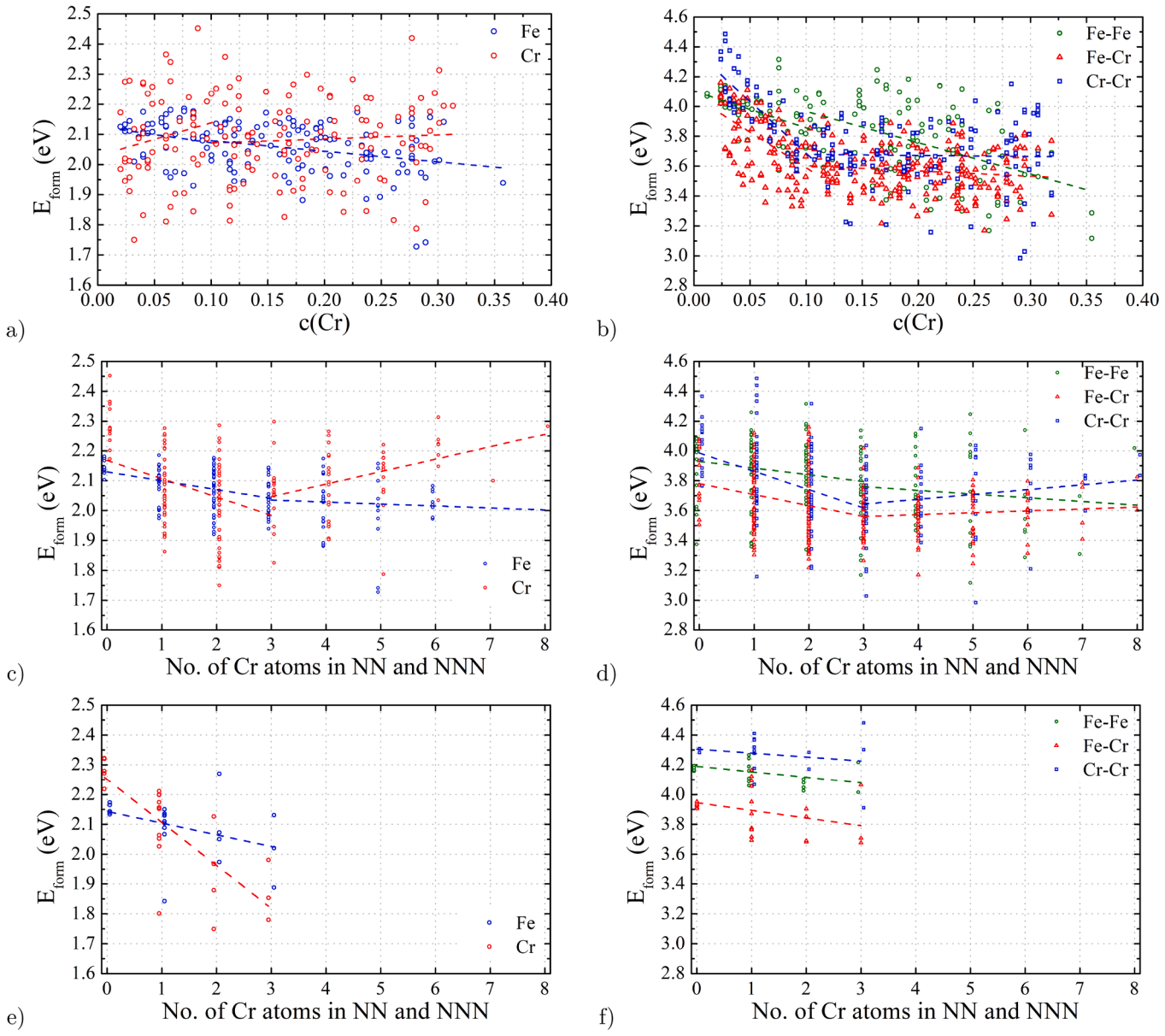

Fig. 4. Formation energy of vacancies (a,c,e) and (b,d,f) SIA dumbbells in random Fe-Cr alloys shown over the entire range of concentrations (a–d) and for an alloy with 5% at. Cr (e,f) plotted as a function of Cr concentration (a,b) and the total number of Cr atoms in the NN and NNN coordination shells of a defect (c–f). Linear trends are indicated by dashed lines (see Table A.2).

comparison of the computed values of elastic parameters with the available experimental data, is given in the Supplementary Materials.

3.3. Elastic dipole and relaxation volume tensors of point defects in bcc Fe and bcc Cr

Elements of elastic dipole tensor P_{ij}, relaxation volume tensor Ω_{ij}, and relaxation volumes Ω_{rel} and Ω^{at}_{rel} of a vacancy as well as Fe-Fe, Fe-Cr, and Cr-Cr $\langle 110 \rangle$ dumbbells in bcc Fe and bcc Cr are listed in Table 1. Relaxation volumes Ω_{rel} are given in Å^3 units, whereas Ω^{at}_{rel} are given in atomic volume units ($\Omega_0 = a^3/2$), where the reference atomic volume $\Omega_0 = 11.345$ Å^3 corresponds to the bcc lattice parameter of $a = 2.831$ Å. In agreement with the analysis given in Ref. [15], P_{ij}, Ω_{ij}, Ω_{rel} and Ω^{at}_{rel} for vacancies are negative in both pure Fe and Cr, whereas for dumbbells they are positive and their magnitudes are significantly larger than those for vacancies. The fact that SIA defects have large relaxation volumes shows that self-interstitial atom defects are primarily responsible for the swelling occurring in these metals under irradiation, as a result of formation of Frenkel vacancy–self-interstitial pairs, and the subsequent clustering of SIA defects [75].

For vacancies in pure metals, all the diagonal elements of elastic dipole tensors and relaxation volume tensors are equal, and the off-diagonal elements vanish. Hence, the elastic properties of vacancies can be described by only one parameter. The values of P_{ij}, Ω_{ij}, and Ω_{rel} are approximately twice as large for vacancies in bcc Cr in comparison with bcc Fe. For example, the relaxation volume of a vacancy in Cr is -6.513 Å^3 and in Fe it is -3.045 Å^3. These values are larger (*i.e.* more negative) than the values found in Ref. [15]. The difference is larger for the vacancy in bcc Cr. This is mainly due to the fact that calculations for bcc Cr in Ref. [15] were performed for the equilibrium lattice parameter of 2.862 Å, whereas all the fixed-volume calculations in this work, including those for bcc Cr, were performed assuming the lattice parameter of bcc Fe of $a = 2.831$ Å.

We note that substitutional atoms in bcc Fe and bcc Cr, namely Cr in Fe, see Fig. 2a), and Fe in Cr (see Fig. 2b), can also be treated using the

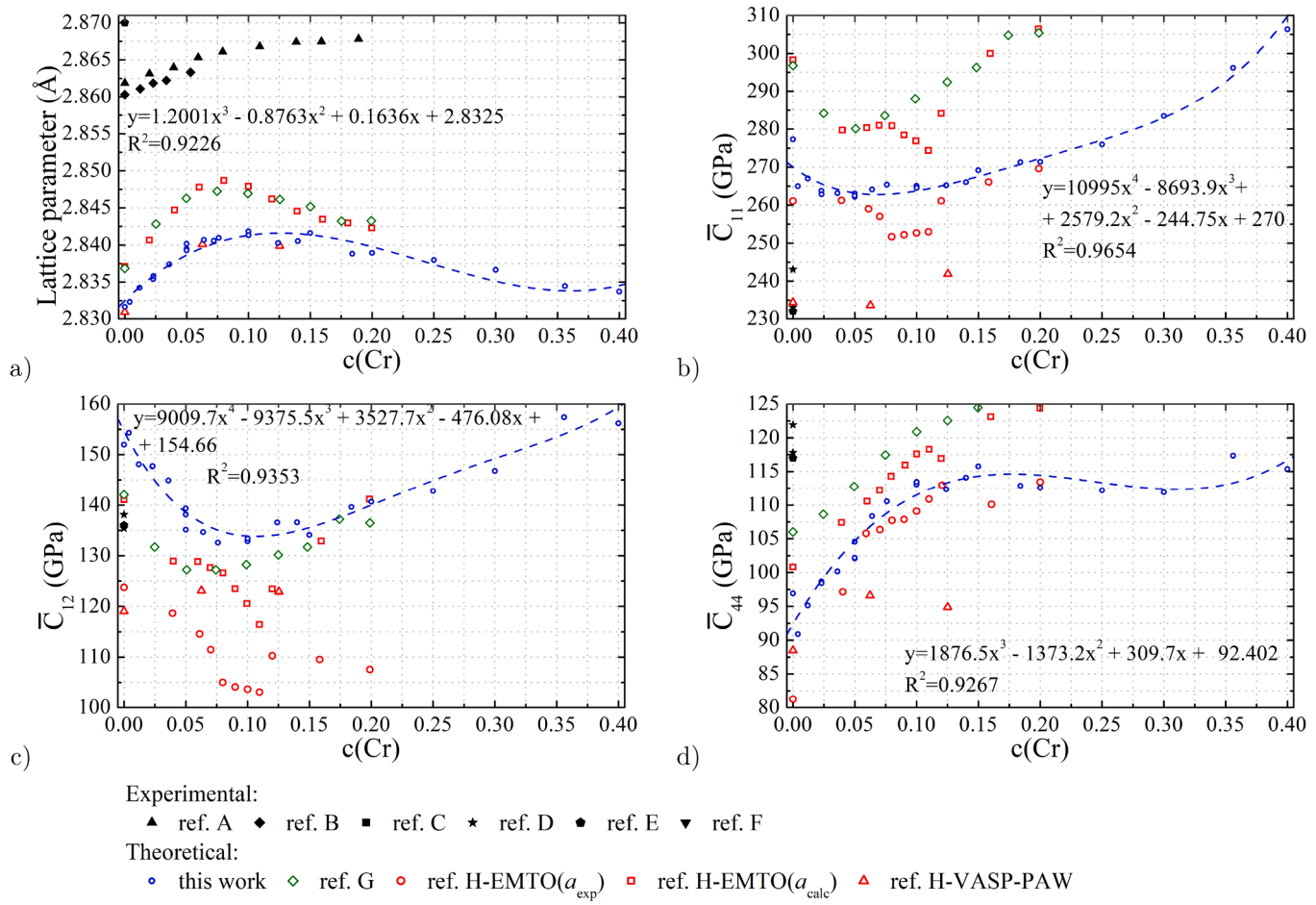

Fig. 5. (a) Average lattice parameter of fully relaxed Fe-Cr structures and average elastic moduli (a) $\overline{C}_{11}$, (b) $\overline{C}_{12}$ and (c) $\overline{C}_{44}$ plotted as functions of Cr content. Experimental: Ref. A [69], Ref. B [70], Ref. C [71], Ref. D [72], Ref. E [73], Ref. F [74]; Theoretical: Ref. G [68], Ref. H [67]. Fitted functions are given in Table A.3.

relaxation volume method formalism developed for point defects. For example, Ω^{at}_{rel} of a substitutional Cr atom in ferromagnetic bcc Fe is equal to 0.184 atomic volume units, which means that its volume is approximately 18% larger than the volume of a host Fe atom. Interestingly, this value is about *four times* larger than the value obtained from the comparison of metallic radii of Fe and Cr, which are 1.26 Å and 1.28 Å, respectively [76]. The origin of the difference is likely related to the magnetic state of a Cr atom, which is different in anti-ferromagnetic bcc Cr and in ferromagnetic bcc Fe matrix. The magnitude of the magnetic moment of a substitutional Cr atom in bcc Fe matrix (1.80 μ_B) is 70% larger than the magnitude of the magnetic moment of a Cr atom in chromium metal, where according to DFT calculations [3] it equals 1.07 μ_B.

We note also that the absolute values of P_{ij}, Ω_{ij}, and Ω_{rel} of a Cr atom in bcc Fe are only approximately 30% smaller than those of a vacancy. It means that elastic distortions caused by a vacancy or a Cr substitutional atom in bcc Fe are broadly similar. The signs of P_{ij}, Ω_{ij}, and Ω_{rel} for a vacancy and substitutional Cr are opposite, Ω_{rel} for a vacancy is negative and Ω_{rel} for a substitutional Cr is positive. The latter is important as it shows that a Cr atom in bcc Fe appears significantly oversized. As a consequence, Cr atoms should be expected to segregate to the outside part of an interstitial dislocation loop where strain is tensile. This is consistent with the interpretation of experimental data obtained using atom probe tomography by Jiao and Was [77], showing that Cr segregates to the outside of an interstitial dislocation loop. It should be noted that the agreement between our calculations and the above experimental results is not fully supported by the DFT results from Ref. [78], where it was found that binding of a Cr atom to a ⟨111⟩ interstitial loop in bcc Fe is insignificant on either the compressive or tensile side of the curved edge dislocation forming the perimeter of an interstitial loop.

As opposed to a Cr atom in bcc Fe, a substitutional Fe atom in bcc Cr has a negative relaxation volume. It means that, similarly to a vacancy, a substitutional Fe atom in bcc Cr produces lattice contraction. The absolute scale of P_{ij}, Ω_{ij}, and Ω_{rel} characterising a Fe atom in bcc chromium matrix is almost ten times smaller than that of a vacancy. For example, Ω^{at}_{rel} for a Fe atom and a vacancy in bcc Cr equals -0.055 and -0.588 atomic volume units, respectively. The relaxation volume of a substitutional Fe atom in Cr matrix is similar to what is expected from the comparison of metallic radii of Fe and Cr [76]. This means that, as opposed to the case of a Cr substitutional atom in bcc Fe matrix, the relaxation volume of a Fe substitutional atom in bcc Cr is not affected by magneto-volume effects.

When treating ⟨110⟩ Fe-Fe, Fe-Cr and Cr-Cr dumbbells (see Fig. 2c–e, respectively) in bcc Fe and Cr, we find that only two diagonal elements of the elastic dipole tensor or the relaxation volume tensor are equal ($P_{22} = P_{33}$ and $\Omega_{22} = \Omega_{33}$). When referring to the specific off-diagonal elements of tensors, we note that the results for ⟨110⟩ dumbbells in this work were computed for dumbbells with [011] orientation. For a Fe-Fe dumbbell in bcc Fe, the first element P_{11} is larger than either P_{22} or P_{33}, whereas the first element is smaller than the other two elements for a Cr-Cr dumbbell in bcc Cr. The P_{11}/P_{22} ratio is 1.21 and 0.78 in the former and latter cases, respectively. This effect is likely caused by the significantly different anisotropy of elastic properties of bcc Fe and bcc Cr, illustrated in Fig. S2b–e in the Supplementary Materials. In bcc Fe and bcc Cr, the lowest and the largest P_{11}/P_{22} ratios are observed for Cr-Cr and Fe-Fe dumbbells, respectively. As opposed to vacancies, all the

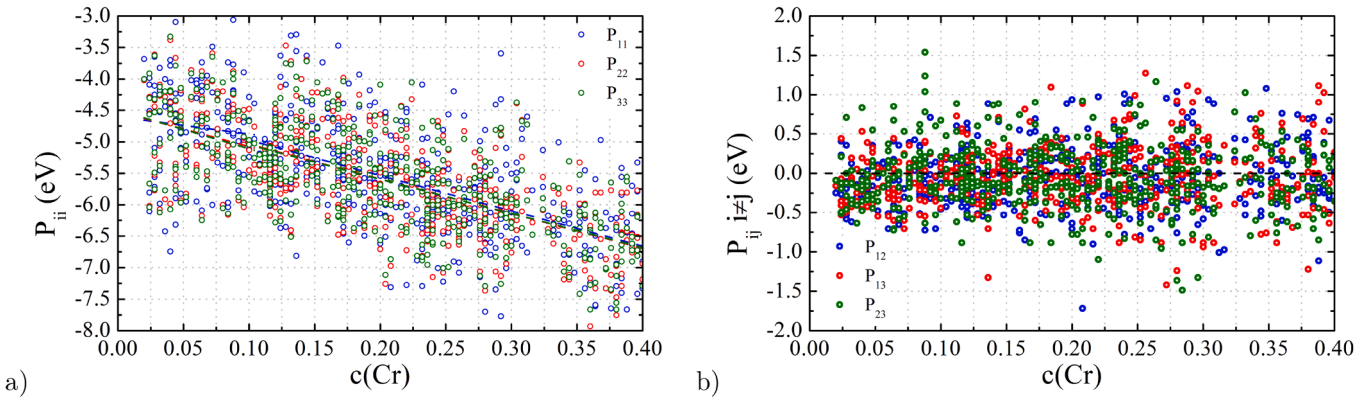

Fig. 6. (a) diagonal and (b) off-diagonal elements of elastic dipole tensor for vacancies on Fe and Cr sites in random Fe-Cr alloy structures. The dashed trend lines equations are given in Table A.4.

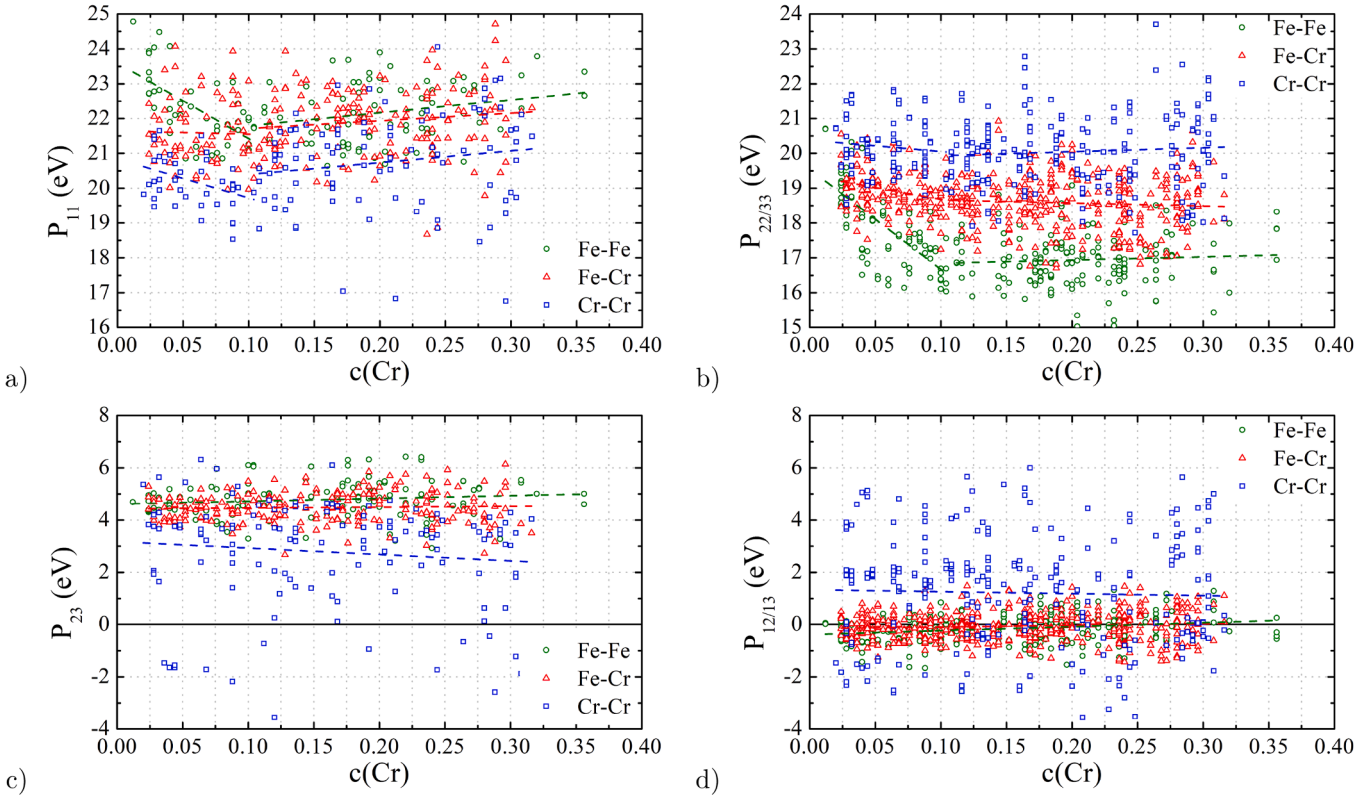

Fig. 7. Elements of elastic dipole tensor (a) P_{11}, (b) P_{22} and P_{33}, (c) P_{23}, and (d) P_{12} and P_{13}, computed for Fe-Fe, Fe-Cr and Cr-Cr [011] dumbbells in random Fe-Cr alloys. The dashed trend lines equations are given in Table A.4.

dumbbells in bcc Fe and Cr have non-vanishing off-diagonal elements P_{23} and Ω_{23} of elastic dipole and relaxation volume tensors. In bcc Fe and bcc Cr, the largest value of P_{23} is found for Cr-Cr dumbbells.

In general, relaxation volumes of dumbbells in bcc Fe are larger than in bcc Cr. For example, the relaxation volume of a Fe-Fe ⟨110⟩ dumbbell in bcc Fe is 18.181 Å^3, which is larger than the relaxation volume of a Cr-Cr dumbbell in bcc Cr, where it is equal to 16.402 Å^3. Finally, we note that the values of P_{ij}, Ω_{ij}, and Ω_{rel} for mixed Fe-Cr dumbbells vary, depending on the type of the atom, Cr or Fe, on the defect site in the pristine structure (see Fig. 3a and b). For example, a Fe-Cr ⟨110⟩ dumbbell on a Fe or a Cr site has the relaxation volume of 18.581 Å^3 and 16.356 Å^3, respectively.

3.4. Elastic dipole tensors and relaxation volumes of point defects in random Fe-Cr alloys

In random Fe-Cr alloys, the elements of P_{ij} and Ω_{ij} depend not only on the type of the defect but also on the atomic configuration of Cr and Fe in its local environment. Due to the random choice of positions of Cr atoms, all the elements of P_{ij} and Ω_{ij} of defects differ from each other and are non-zero, even for vacancies – whereas in pure metals, because of the cubic symmetry, we find that $P_{11} = P_{22} = P_{33}$ and $P_{12} = P_{23} = P_{31} = 0$. Figs. 6 and 7 show that the values of P_{ij} for vacancies and dumbbells exhibit significant scattering. However, similarly to the data for defects in pure metals, there are notable identifiable trends that we discuss below.

For vacancies, the magnitudes of P_{11}, P_{22} and P_{33} are notably larger than those of P_{12}, P_{23} and P_{31}, and the mean values of the off-diagonal

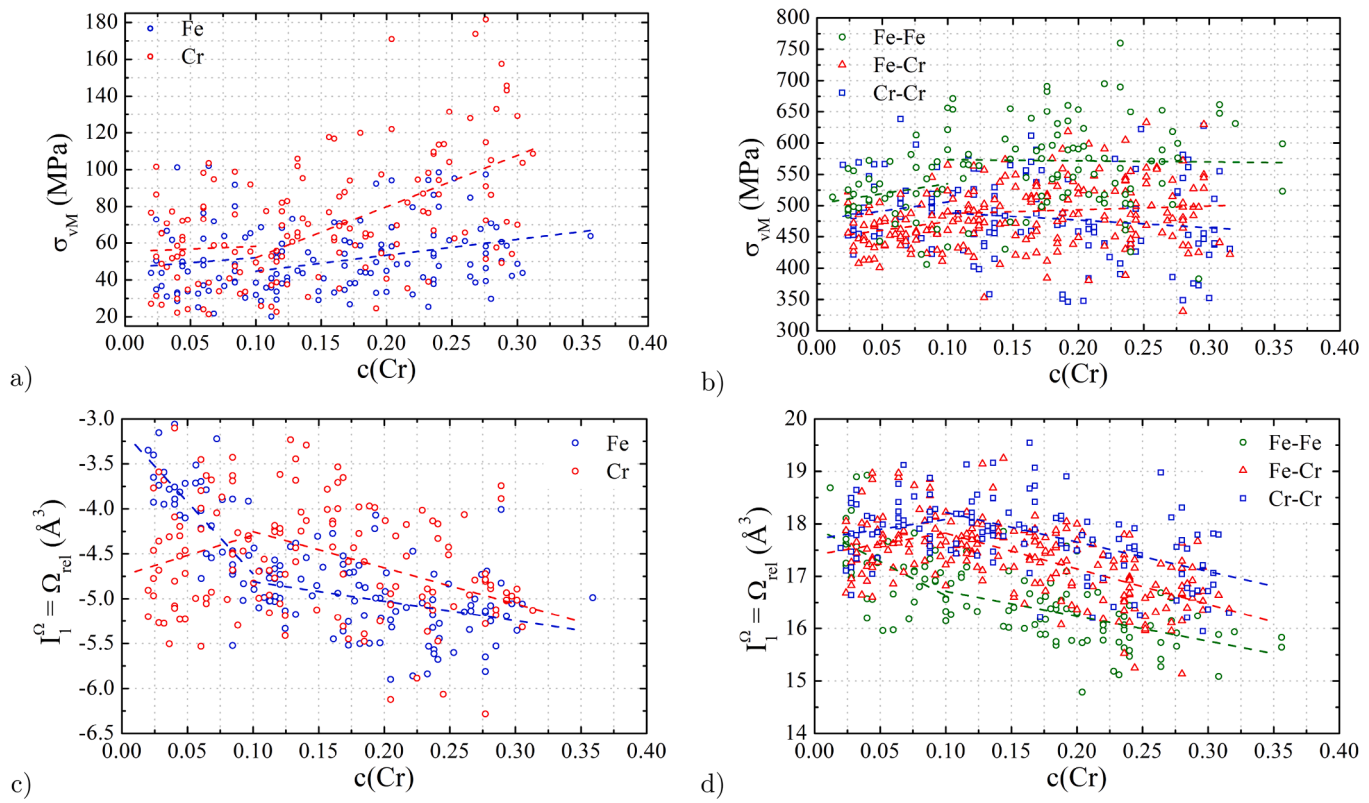

Fig. 8. Von Mises stresses obtained form the invariants of elastic dipole tensors I_1^P and I_2^P (a,b) and first invariants of relaxation volume tensor I_1^Ω, computed for (a,c) vacancies on Fe and Cr sites and (b,d) Fe-Fe, Fe-Cr and Cr-Cr dumbbells in random Fe-Cr alloys. Calculations were performed using a $5 \times 5 \times 5$ supercell with volume of 2836.15 Å^3, corresponding to the average volume concentration of defects of $3.526 \cdot 10^{26}$ m^{-3}. The dashed trend lines equations are given in Table A.5.

elements of the dipole tensor are very close to zero, see Fig. 6. This is expected, and is consistent with the argument given in Ref. [20] that averaging over configurations generally gives rise to the isotropic form of dipole and relaxation volume tensors. For dumbbells, as in the case of pure metals, values of P_{22} and P_{33} are usually similar, whereas P_{11} can be either smaller or larger than P_{22} and P_{33}, cf. Fig. 7a and b.

Similarly to pure bcc Fe and Cr, the dipole tensors of ⟨110⟩ Fe-Fe and Fe-Cr dumbbells are characterised by a significantly larger value of P_{11} in comparison with P_{22} and P_{33} over the entire range of alloy compositions considered here. As before, calculations for ⟨110⟩ dumbbells were performed for the [011] orientation. On the other hand, Cr-Cr dumbbells are characterised by notably smaller P_{11} values, and larger P_{22} and P_{33} values, than Fe-Fe and Fe-Cr dumbbells. As a result, Cr-Cr dumbbells have the P_{11}/P_{22} ratio much closer to unity than Fe-Fe and Fe-Cr dumbbells.

The fact that the values of P_{11}, P_{22} and P_{33} for Cr-Cr dumbbells are similar does not mean that the elastic field of these defects is isotropic. The dipole tensor of every dumbbell defect has large off-diagonal terms. The main difference between Fe-Fe, Fe-Cr and Cr-Cr dumbbells with the [011] orientation is that the two former ones have only one visibly non-zero off-diagonal P_{ij} element, namely P_{23}, and the mean values of P_{12} and P_{31} are close to zero, whereas the latter one often has all the off-diagonal elements that are large. The values of these off-diagonal elements for Cr-Cr dumbbells also fluctuate stronger than those for Fe-Fe and Fe-Cr dumbbells. This effect may be related to the fact that the direction of a Cr-Cr dumbbell is not necessarily close to [011] as it is the case for Fe-Fe and Fe-Cr dumbbells. For example, the most stable Cr-Cr dumbbell in pure Cr is symmetry broken [17] and its orientation is close to $\langle 11\xi \rangle$. Orientations of dumbbells in Fe-Cr alloys will be discussed in Section 4.1.

To understand the changes exhibited by P_{ij} as a function of Cr content, we computed the trends shown in Figs. 6 and 7. For vacancies, P_{11}, P_{22} and P_{33} decrease as a function of Cr concentration. At low Cr concentration, these values approximately approach the value observed for a vacancy in pure bcc Fe. Equations for the trend lines are given in Table A.4 in Appendix.

The data ranges for Fe-Fe, Fe-Cr and Cr-Cr dumbbells are divided into two categories: those corresponding to alloy compositions below and above 10% at. Cr. The trend lines for these two concentration ranges may be significantly different. For example, the mean value of P_{11} for dumbbells in alloys with Cr concentration lower than 10% at. Cr decreases with Cr content whereas for larger Cr concentrations it increases. In the low Cr concentration limit, the steepest and slightest slopes are observed for the Fe-Fe and Fe-Cr dumbbells, respectively. At a low Cr concentration, P_{11} is close to the value found for these defects formed on a Cr site in bcc Fe matrix. The mean values of P_{22} and P_{33} for Fe-Cr and Cr-Cr dumbbells are almost constant over the range of concentrations studied here, whereas for Fe-Fe, they decrease notably as a function of Cr content up to the Cr concentration close to approx. 10% at.

To characterise elastic dipole and relaxation volume tensors of point defects in Fe-Cr alloys in a way that is independent of rotations of coordinates, we have computed invariants of the two tensors. Invariants of elastic dipole tensors I_1^P, I_2^P and I_3^P are shown in Fig. S3 and the trend lines are given in Table S3, whereas the invariants of relaxation volume tensors I_1^Ω, I_2^Ω and I_3^Ω are shown in Fig. S4 and the trend lines are given in Table S3 in the Supplementary Materials. Although the invariants of elastic dipole and relaxation volume tensor can be useful for the development of higher scale models, in Fig. 8 we only show quantities that can be readily observed, the von Mises stresses produced in the material by the distributed defects, and the relaxation volumes of defects.

Eq. (13) shows that the von Mises stress computed from invariants I_1^P and I_2^P depend on the volume of the simulation cell or, in other words, on the density of defects periodically and homogeneously distributed in the

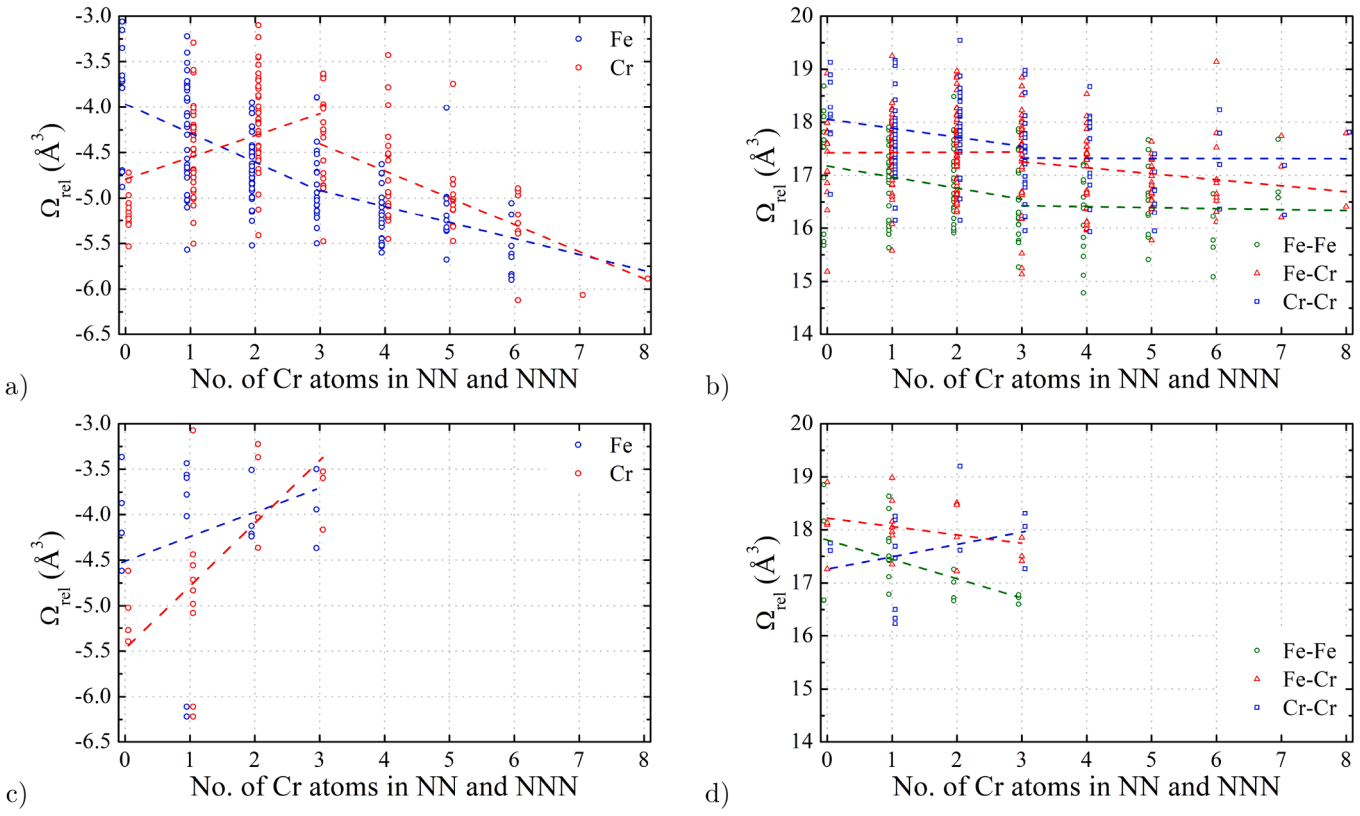

Fig. 9. Relaxation volumes of vacancies on Fe and Cr sites (a,c) and dumbbells (b,d) in random Fe-Cr alloys plotted over the entire range of compositions (a,b) and for the alloy containing 5% at. Cr (c,d), as a function of the total number of Cr atoms in the NN and NNN coordination shells of a defect. Linear trends are indicated by dashed lines (see Table A.6).

material. The values shown in the Fig. 8a and b were computed using a $5 \times 5 \times 5$ supercell with the volume of 2836.15 Å^3, corresponding to the volume density of defects of $3.526 \cdot 10^{26}$ m^{-3}. Values of the von Mises stress corresponding to any other density of defects can be readily computed by scaling the values given in Fig. 8 linearly to any other density of defects.

Fig. 8a shows that the von Mises stress (σ_{vM}) generated by vacancies, homogeneously and periodically distributed in specific configurations of Fe-Cr alloys, exhibit considerable fluctuations. The stress developing in the material depends on the composition of the alloy and the location of a vacancy in the alloy structure. In alloys containing less that 10% at. Cr, σ_{vM} varies between 20 and 100 MPa. The mean value is close to 50 MPa, and it appears that vacancies located at Cr sites produce higher tensile stresses in the material. In alloys containing higher amount of Cr, σ_{vM} fluctuates even stronger.

σ_{vM} for SIA dumbbells also exhibits different behaviour below and above 10% at. Cr. At lower Cr concentrations, values of σ_{vM} are between 400 and 600 MPa, whereas at larger Cr concentration the results are more scattered and values of σ_{vM} are between 350 and 700 MPa. Mean values of σ_{vM} for Fe-Cr and Cr-Cr dumbbells do not change significantly with Cr content and over the entire range of compositions they vary between 450 and 500 MPa. Values of σ_{vM} for Fe-Fe SIAs are larger than for Fe-Cr and Cr-Cr dumbbells. At small Cr concentration, the mean value of σ_{vM} for Fe-Fe dumbbells is close to 500 MPa and it increases with Cr content. For alloys with Cr concentration above 10%, the mean value of σ_{vM} is larger, and is close to 575 MPa, and it does not change appreciably with Cr content.

Relaxation volumes of vacancies and dumbbells in random Fe-Cr alloys, computed from the first invariants of the corresponding Ω_{ij} tensors, are shown in Fig. 8c and d, respectively. Relaxation volumes of vacancies in random Fe-Cr alloys are in general more negative than the volume of a vacancy in pure bcc Fe. Even in the low Cr concentration limit the mean value of Ω_{rel} of a vacancy is -2.4 Å^3, which is approximately 50% more negative than Ω_{rel} for a vacancy in bcc Fe. Fig. 8c shows values of mean relaxation volumes computed for vacancies located at Fe or Cr sites. The results are noticeably different below and above 10% at. Cr concentration, and therefore the trend lines are described more accurately using two linear fits, one below and another above 10% at. Cr. The most rapid decrease of the mean relaxation volume as a function of Cr content is observed for vacancies on a Fe site at low Cr concentration, whereas Ω_{rel} of a vacancy on a Cr site increases as a function of Cr content. For Cr concentrations above 10% at. Cr, Ω_{rel} of a vacancy on both sites decreases as a function of Cr content but the slope of the fitted line for a vacancy on a Cr site is steeper.

Relaxation volumes of dumbbells are all positive, and their magnitudes are much larger than those of vacancies (see Fig. 8d). Results for Fe-Fe, Fe-Cr and Cr-Cr dumbbells are different above and below approx. 10% at. Cr. For Cr concentration below 10% at. Cr, the mean values of Ω_{rel} for Fe-Cr and Cr-Cr SIAs increases, whereas for Fe-Fe decrease rapidly as a function of Cr content. As a result, the mean values of Ω_{rel} for Fe-Fe dumbbells are the largest at very small Cr concentrations (below approx. 2% at. Cr) and the lowest for larger Cr concentrations. At a low Cr concentration, the mean values of Ω_{rel} for the three types of dumbbells are similar to the values computed for pure bcc Fe (results for Fe-Cr dumbbells in Fe-Cr alloys are closer to the values for a dumbbell formed on a Cr site than on a Fe site in bcc Fe matrix). For Cr concentrations above approx. 10% Cr, Ω_{rel} for all the three types of dumbbells decreases as a function of Cr content, in agreement with that Ω_{rel} for these dumbbells in bcc Cr is notably smaller than in bcc Fe. The slopes of the fitted lines in each case are similar.

Equations for the trend lines describing how the von Mises stresses and relaxation volumes computed for point defects vary as a function of Cr concentration are given in Table A.5 in Appendix. Equations for the trend lines for invariants I_1^P, I_2^P, I_3^P, I_1^Ω, I_2^Ω and I_3^Ω are given in Table S3

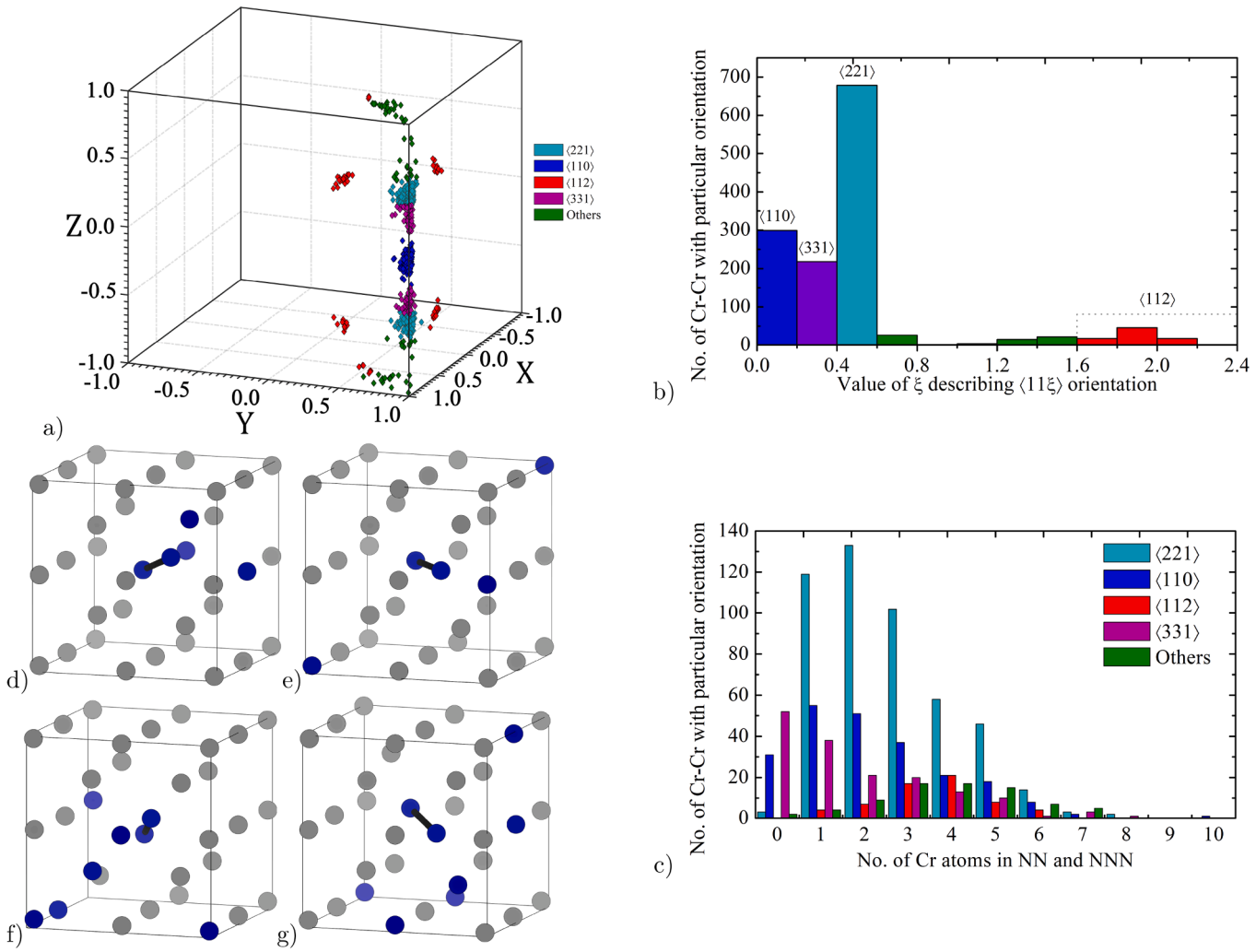

Fig. 10. (a) Schematic representation of Cr-Cr dumbbell orientations – the orientations have been normalised and presented in such a way that the equivalent directions have positive values on X and Y axes, (b) the number of $\langle 11\xi \rangle$ Cr-Cr dumbbells as a function of parameter ξ and (c) the number of Cr-Cr dumbbells in a particular orientation as a function of the number of Cr atoms in the NN and NNN coordination shell of a defect. Examples of alloy configurations in the local environment of a Cr-Cr dumbbell adopting specific orientations: (d) $\langle 221 \rangle$, (e) $\langle 110 \rangle$, (f) $\langle 112 \rangle$, (g) $\langle 331 \rangle$. Fe and Cr atoms are shown by grey and blue spheres, respectively.

in the Supplementary Materials.

Comparison of relaxation volumes of vacancies and dumbbells in random Fe-Cr alloys for the entire range of concentrations and for the alloy with 5% at. Cr as a function of number of Cr atoms in the local environment of a defect is given in Fig. 9. As in Fig. 4, point defects in Fe-5%Cr alloys are surrounded by up to 3 Cr atoms in the NN and NNN shells. To compare results with those computed for other Fe-Cr alloys, the latter ones have been separated into two groups: for point defects with N_{Cr}^{def} smaller and larger than 3.

Results for the Fe-5%Cr alloy and for all the other alloys show that the mean relaxation volume of a vacancy on a Fe site is larger than that on a Cr site if N_{Cr}^{def} equals 0 and 1, and smaller if N_{Cr}^{def} equals 2 and 3. In the group with the small number of Cr atoms in the local environment of a defect, Ω_{rel} on a Cr site decreases with increasing N_{Cr}^{def} for both alloys. However, Ω_{rel} for a vacancy on a Fe site, averaged over all the alloys, decreases as a function of N_{Cr}^{def} whereas it slightly increases in the Fe-5% Cr alloy. In the region with N_{Cr}^{def} larger than 3, Ω_{rel} decreases with increasing N_{Cr}^{def} for vacancies both on a Fe site and on a Cr site, which agrees with the results presented as a function of Cr concentration, cf. Figs. 9a and 8c.

The trends describing mean relaxation volumes of Fe-Fe and Fe-Cr dumbbells as functions of N_{Cr}^{def} are generally similar in the Fe-5%Cr alloy and in all the other alloys, however the mean values obtained for the Fe-5%Cr alloy are approx. 0.5 Å^3 larger, see Fig. 9a and c. Similarly to the formation energies, the most notable difference between the groups of alloys is observed for Cr-Cr dumbbells – the mean values for a Fe-5%Cr alloy increase whereas those averaged over all the alloys decrease as a function of the number of Cr atoms in NN and NNN around a Cr-Cr dumbbell. The trends for the mean relaxation volumes of Fe-Fe and Cr-Cr dumbbells for N_{Cr}^{def} larger than 3 are almost constant whereas those for Fe-Cr slightly decrease with the number of Cr atoms in the nearest neighbour shells. Equations for the trend lines describing mean relaxation volumes of point defect as functions of N_{Cr}^{def} are given in Table A.6 in Appendix.

4. Discussion

4.1. The orientation of dumbbells

Orientations of SIA, defined by the direction of the vector connecting the two central atoms forming a dumbbell defect, and explored in the calculations, are schematically shown – a Cr-Cr type – in Fig. 10a. Both

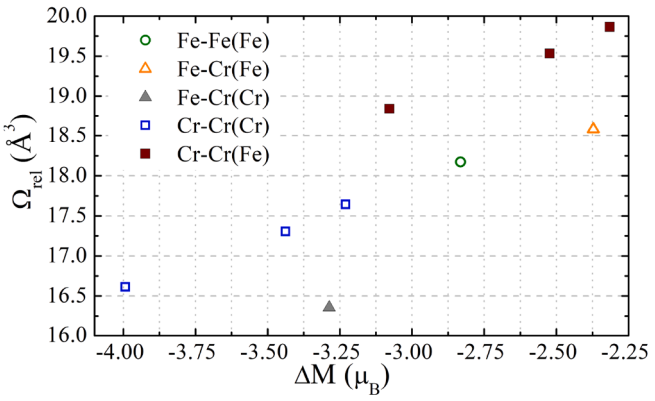

Fig. 11. Relaxation volumes of dumbbells in bcc Fe matrix plotted as a function of the change in the magnitude of the total magnetic moment in the supercell associated with the formation of a defect.

Fe-Fe and Fe-Cr dumbbells adopt a ⟨110⟩ orientation after relaxation. This is similar to the orientation of a dumbbell defect in pure bcc Fe, where it adopts a ⟨110⟩ orientation [18,79,80]. Variation of directions of Cr-Cr dumbbells is much larger, see Fig. 10a. In general, most orientations can be classified as an ⟨11ξ⟩ orientation where ξ spans the interval from 0.0 to 2.4. We have combined possible orientations of defects into five different groups, corresponding to different intervals of parameter ξ, namely ⟨110⟩ ($0.0 < \xi < 0.2$), ⟨331⟩ ($0.2 < \xi < 0.4$), ⟨221⟩ ($0.4 < \xi < 0.6$), ⟨112⟩ ($1.6 < \xi < 2.4$) orientations as well as others, see Fig. 10b. The number of dumbbells adopting a particular orientation as a function of the number of Cr atoms in the 1st and 2nd coordination shells around a defect is shown in Fig. 10c. Examples of alloy configurations in the local environment of a Cr-Cr dumbbell adopting a particular orientation are shown in Fig. 10d–g. The most common direction of a Cr-Cr dumbbell is ⟨221⟩ (about 48.0% of all Cr-Cr dumbbells), however this fraction decreases as the number of Cr atoms in the local environment of a dumbbell increases. The prevalence of the ⟨221⟩ direction (indicated by the aquamarine colour in Fig. 10b) of Cr-Cr agrees with the earlier results by Klaver *et al.* [26]. For the configurations containing no Cr atoms in the 1st and 2nd coordination shells around a self-interstitial defect, the ⟨331⟩ (purple) and ⟨110⟩ (navy blue) orientations are more common (for example, ⟨331⟩ and ⟨110⟩ orientations represent 59.1% and 35.2% of all the directions of dumbbells that have no Cr atoms in their vicinity). The occurrence of dumbbells with orientations ⟨112⟩ (indicated by the red colour in Fig. 10b) as well as with orientations with higher crystallographic indices, the so-called 'thers' (green), increases with the number of Cr atoms in the local environment of a defect.

4.2. Magneto-volume effects in Fe-Cr alloys

To understand the origin of differences between the relaxation volumes of dumbbells on Fe and Cr sites in bcc Fe, values of Ω_{rel} were correlated with the variation of the magnitude of the magnetic moment in the supercell ΔM caused by the defect. Fig. 11 shows that smaller values of relaxation volumes of dumbbells are correlated with ΔM being more negative. In particular, Ω_{rel} of a ⟨110⟩ Fe-Cr dumbbell on a Fe site (18.581 Å^3) is larger than that of a ⟨110⟩ Fe-Fe dumbbell on a Fe site (18.171 Å^3) since the sum of magnitudes of magnetic moments for the former structure is almost 0.5 μ_B larger. This suggests that magnetism is a significant factor affecting structural relaxation and hence relaxation volumes of defects in Fe-Cr alloys. The difference in magnetic properties between the structures containing Fe-Fe and Fe-Cr dumbbells is caused mainly by the differences in magnetic moments of atoms forming the dumbbells, which agrees with Refs. [29,34,42].

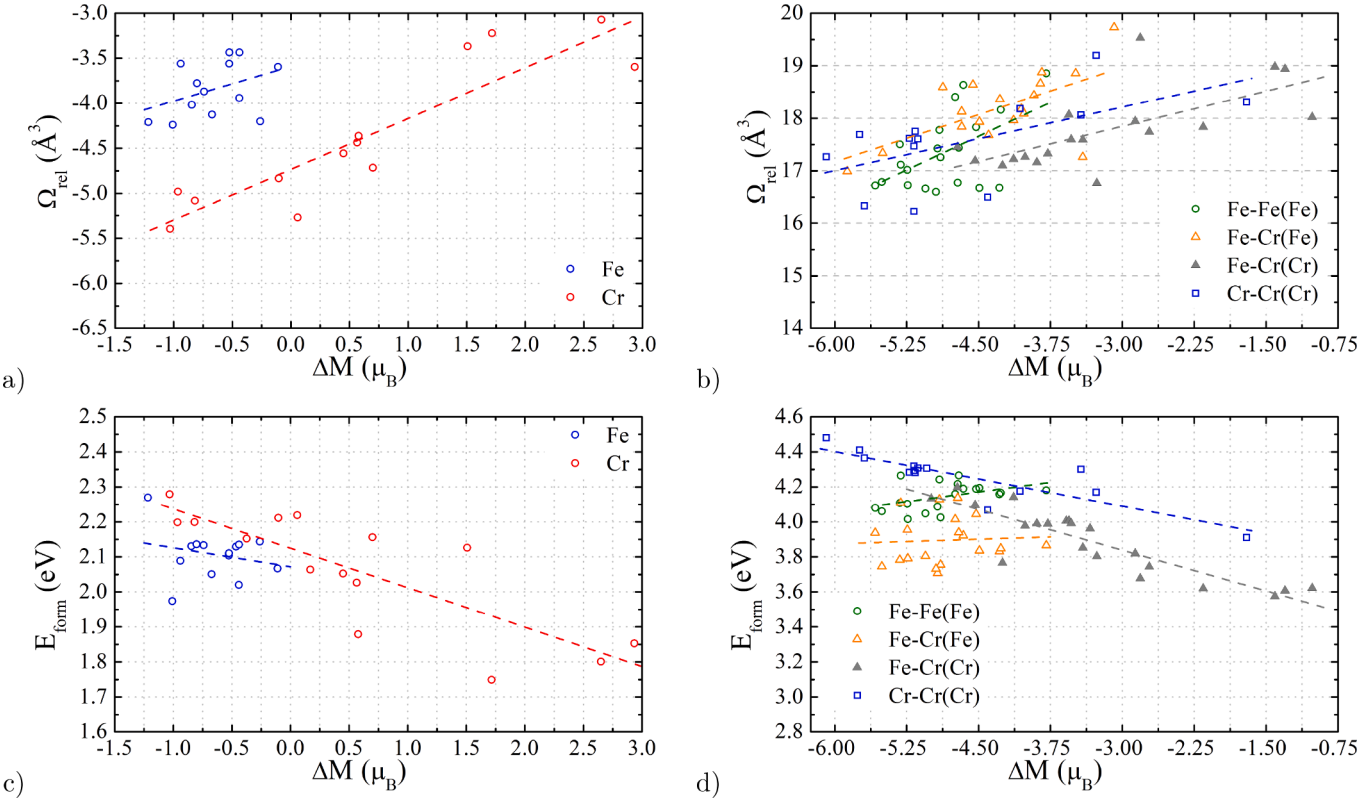

Fig. 12. Relaxation volumes (a,b) and formation energies (c,d) of vacancies on Fe and Cr sites (a,c) and dumbbells (b,d) in random Fe-Cr alloys for the alloy with 5% at. Cr as a function of variation of the magnitude of the total magnetic moment in the supercell, caused by a defect. Linear trends are indicated by dashed lines (their equations and R^2 values are given in Tables A.2 and A.6).

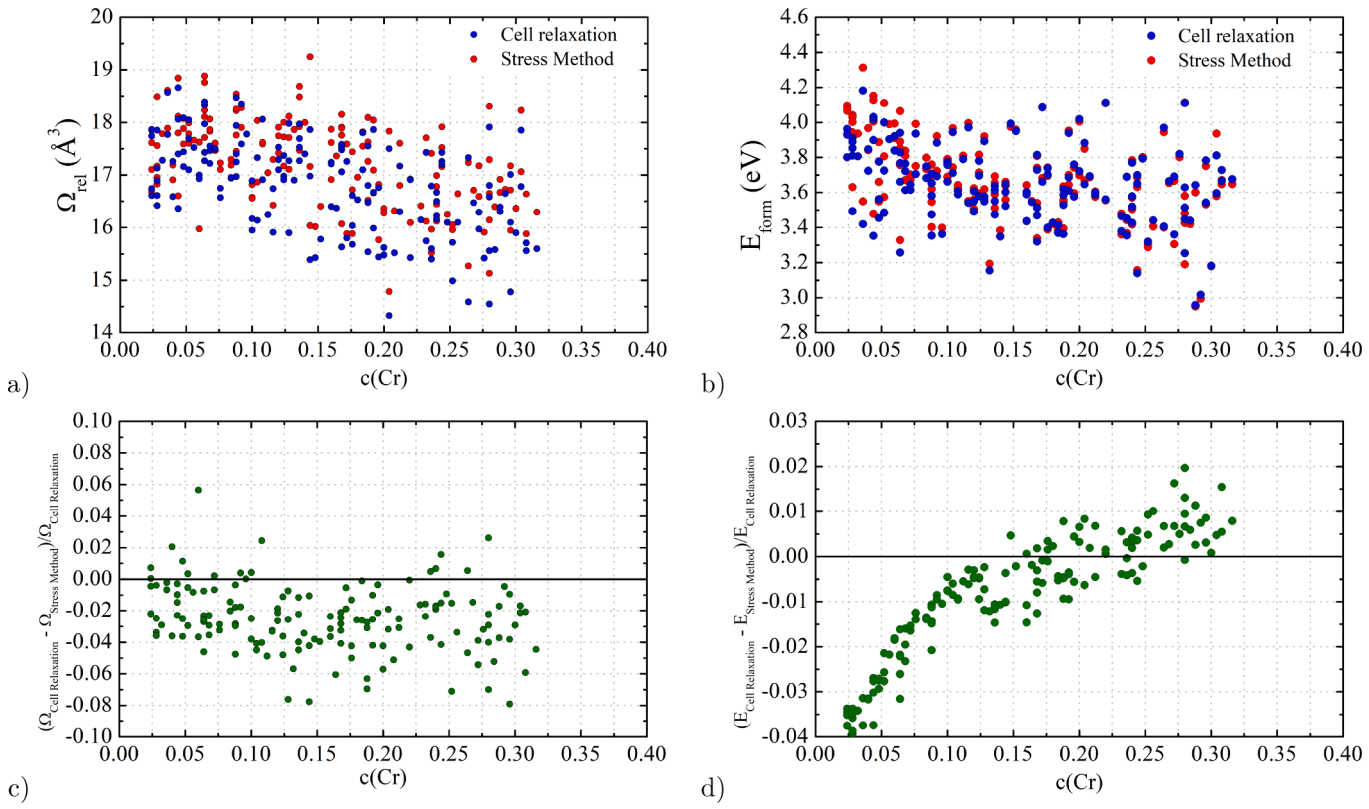

Fig. 13. Comparison of (a) relaxation volumes and (b) formation energies of SIA dumbbells evaluated using the stress and cell relaxation methods, and the relative difference between (c) relaxation volumes and (d) formation energies computed using both methods.

In a ⟨110⟩Fe-Fe SIA dumbbell, the magnetic moments of Fe atoms are small ($-0.207\,\mu_B$) and they are ordered antiferromagnetically with respect to other Fe atoms. In a ⟨110⟩Fe-Cr dumbbell the magnetic moment of Fe is larger ($0.326\,\mu_B$) and its ordered ferromagnetically with respect to other Fe moments, and antiferromagnetically with respect to the moment of the Cr atom in the dumbbell, which has a notably larger magnitude of magnetic moment ($-0.946\,\mu_B$). Magnetic moments of atoms in Fe-Fe and Fe-Cr dumbbells in bcc Fe are in agreement with the values given in Refs. [34,66]. Magnetic moments of Cr atoms in a ⟨11ξ⟩Cr-Cr dumbbell are $-0.347\,\mu_B$, and both are aligned antiferromagnetically with respect to the magnetic moments of Fe atoms.

Similarly to dumbbells in Fe matrix, there is a correlation between the relaxation volume of a defect and the variation of the magnitude of the total magnetic moment in the supercell caused by a defect (ΔM), see Fig. 12a–d (equations of trend lines and R^2 values are given in Tables A.2 and A.6). For vacancies and dumbbells, Ω_{rel} increases as a function of ΔM. As in bcc Fe matrix, Fe-Cr dumbbells on a Fe site in a Fe-5%Cr alloy have larger magnitudes of magnetic moments and consequently larger relaxation volumes than Fe-Fe dumbbells on a Fe site. Slopes of trend lines for dumbbells indicate that the largest and smallest variations of Ω_{rel} with ΔM are observed for Fe-Fe and Cr-Cr dumbbells, respectively. Slopes of trend lines for vacancies and Fe-Cr do not change significantly depending on the lattice site where a defect is formed. Values of Ω_{rel} for defects formed on Cr sites are generally smaller.

Variation of magnitudes of magnetic moments associated with a defect also influences the formation energy of a defect. Fig. 12c shows that E_{form} of vacancies decreases with increasing ΔM. Comparing the results presented in Fig. 12a and c, we see a correlation between Ω_{rel} and E_{form} of vacancies, indeed E_{form} decreases as the absolute value of Ω_{rel} decreases. According to Fig. 12d, values of E_{form} for Fe-Cr and Cr-Cr dumbbells on a Cr site decrease whereas those for Fe-Fe and Fe-Cr dumbbell on a Fe site slightly increase as a function of ΔM. At the same time, a comparison of Fig. 12b and d does not show any clear correlation between Ω_{rel} and E_{form} for dumbbells in Fe-Cr alloys.

4.3. Comparison of the cell relaxation and stress methods

A comparison of results obtained using the stress and full cell relaxation methods for 160 random Fe-Cr structures is shown in Fig. 13. Both approaches show that relaxation volumes and formation energies of dumbbells in random Fe-Cr alloys decrease with Cr content, see Fig. 13a and b. The stress method predicts somewhat larger values of relaxation volumes and formation energies than the cell relaxation method, exhibiting a correlation between E_{form} and Ω_{rel}. The relaxation volumes of defects computed using the stress method are on average 2.5% larger, however there are a few structures where they are more than 5% larger than the values derived using the cell relaxation method, see Fig. 13c. Fig. 13d shows that the relative difference between formation energies of defects E_{form} deduced using the stress and cell relaxation methods varies as a function of Cr content. Similarly to the majority of results given in sections above, the relative formation energy difference exhibits different behaviour in the two composition intervals, above and below 10% at. Cr. Above 10% at. Cr, the relative formation energy difference increases slowly as a function of Cr content. Values E_{form} obtained using the stress method do not differ in general by more than 2% in comparison with values computed using the full relaxation method, and the average relative formation energy difference in that interval of Cr concentrations is almost equal to zero. For Cr concentrations below 10%, the overestimation of E_{form} obtained using the stress method in comparison with that computed using the cell relaxation method increases towards low Cr content, reaching approximately −4% for alloys containing approximately 3% at. Cr. It is worth noting that the elastic correction, implemented following Refs. [12–14,16,21], improves agreement between the results obtained using both methods. Still, the use of elastic correction often proves insufficient, as it was found for defect clusters in Tungsten [43,44].

There are several reasons that might be responsible for the discrepancy. The lattice parameter used in the fixed volume calculations may

Table A.2
Equations for the trend lines of chemical potentials ($\mu_{Fe/Cr}$ in eV), formation energies (E_{form} in eV) of vacancies and dumbbells in random Fe-Cr alloys as a function of the chromium concentration ($c(Cr)$) or the number of Cr atoms in the vicinity of a defect (N_{Cr}^{def}) and formation energies (E_{form} in eV) as a function of change of magnitudes of magnetic moments (ΔM in μ_B) caused by a defect for the alloy with 5% at. Cr.

Parameter	Variation as a function of the variable in square brackets, denoted here as x	Parameter	Variation as a function of the variable in square brackets, denoted here as x
	Chemical potentials (see Fig. 1)		
$\mu_{Fe}[c(Cr)]$	$y = -0.0088x - 8.3193$	$\mu_{Cr}[c(Cr)]$	$y = \begin{cases} 3.8323x - 9.606 & \text{for } x \leqslant 0.1 \\ -0.2328x - 9.2251 & \text{for } x > 0.1 \end{cases}$
	Formation energies of vacancies (see Fig. 4a and c)		
$E_{form}^{vac(Fe)}[c(Cr)]$	$y = \begin{cases} -0.5371x + 2.1263 & \text{for } x \leqslant 0.1 \\ -0.3504x + 2.1144 & \text{for } x > 0.1 \end{cases}$	$E_{form}^{vac(Fe)}[N_{Cr}^{def}]$	$y = \begin{cases} -0.0294x + 2.1291 & \text{for } x \leqslant 3 \\ -0.0066x + 2.055 & \text{for } x \geqslant 3 \end{cases}$
$E_{form}^{vac(Cr)}[c(Cr)]$	$y = \begin{cases} 1.09397x + 2.02881 & \text{for } x \leqslant 0.1 \\ 0.13367x + 2.05817 & \text{for } x > 0.1 \end{cases}$	$E_{form}^{vac(Cr)}[N_{Cr}^{def}]$	$y = \begin{cases} -0.0613x + 2.168 & \text{for } x \leqslant 3 \\ 0.0418x + 1.9212 & \text{for } x \geqslant 3 \end{cases}$
	Formation energies of dumbbells (see Fig. 4b and d)		
$E_{form}^{Fe\text{-}Fe}[c(Cr)]$	$y = \begin{cases} -2.47363x + 4.10369 & \text{for } x \leqslant 0.1 \\ -2.10125x + 4.17765 & \text{for } x > 0.1 \end{cases}$	$E_{form}^{Fe\text{-}Fe}[N_{Cr}^{def}]$	$y = \begin{cases} -0.0447x + 3.929 & \text{for } x \leqslant 3 \\ -0.0248x + 3.8344 & \text{for } x \geqslant 3 \end{cases}$
$E_{form}^{Fe\text{-}Cr}[c(Cr)]$	$y = \begin{cases} -4.7541x + 4.06472 & \text{for } x \leqslant 0.1 \\ -0.34985x + 3.63797 & \text{for } x > 0.1 \end{cases}$	$E_{form}^{Fe\text{-}Cr}[N_{Cr}^{def}]$	$y = \begin{cases} -0.0731x + 3.78 & \text{for } x \leqslant 3 \\ 0.0125x + 3.5232 & \text{for } x \geqslant 3 \end{cases}$
$E_{form}^{Cr\text{-}Cr}[c(Cr)]$	$y = \begin{cases} -6.92687x + 4.37945 & \text{for } x \leqslant 0.1 \\ -0.07179x + 3.68609 & \text{for } x > 0.1 \end{cases}$	$E_{form}^{Cr\text{-}Cr}[N_{Cr}^{def}]$	$y = \begin{cases} -0.1225x + 3.985 & \text{for } x \leqslant 3 \\ 0.0322x + 3.5469 & \text{for } x \geqslant 3 \end{cases}$
	Formation energies of vacancies in alloy with 5% at. Cr (see Figs. 4e and 12c)		
$E_{form}^{vac(Fe)}[N_{Cr}^{def}]$	$y = -0.0394x + 2.1451$	$E_{form}^{vac(Fe)}[\Delta M]$	$y = -0.054x + 2.072$, $R^2 = 0.057$
$E_{form}^{vac(Cr)}[N_{Cr}^{def}]$	$y = -0.1438x + 2.2508$	$E_{form}^{vac(Cr)}[\Delta M]$	$y = -0.113x + 2.125$, $R^2 = 0.663$
	Formation energies of dumbbells in alloy with 5% at. Cr (see Figs. 4f and 12d)		
$E_{form}^{Fe\text{-}Fe}[N_{Cr}^{def}]$	$y = -0.0365x + 4.1879$	$E_{form}^{Fe\text{-}Fe(Fe)}[\Delta M]$	$y = 0.073x + 4.501$, $R^2 = 0.187$
		$E_{form}^{Fe\text{-}Cr(Fe)}[\Delta M]$	$y = 0.0176x + 3.9803$, $R^2 = 0.0034$
$E_{form}^{Fe\text{-}Cr}[N_{Cr}^{def}]$	$y = -0.0504x + 3.942$	$E_{form}^{Fe\text{-}Cr(Cr)}[\Delta M]$	$y = -0.1552x + 3.3731$, $R^2 = 0.7784$
$E_{form}^{Cr\text{-}Cr}[N_{Cr}^{def}]$	$y = -0.026x + 4.3029$	$E_{form}^{Cr\text{-}Cr(Cr)}[\Delta M]$	$y = -0.104x + 3.778$, $R^2 = 0.738$

Table A.3
Equations for the fitted curves of average lattice parameter (a in Å), average elastic moduli ($\overline{C}_{11}$, $\overline{C}_{12}$, $\overline{C}_{44}$ in GPa) as a function of chromium concentration ($c(Cr)$) of fully relaxed random Fe-Cr alloy structures (see Fig. 5a–d).

Parameter	Variation as a function of the variable in square brackets, denoted here as x	Parameter	Variation as a function of the variable in square brackets, denoted here as x
$a[c(Cr)]$	$y = 1.2001x^3 - 0.8763x^2 + 0.1636x + 2.8325$	$\overline{C}_{11}[c(Cr)]$	$y = 10995x^4 - 8693.9x^3 + 2579.2x^2 - 244.75x + 270$
$\overline{C}_{12}[c(Cr)]$	$y = 9009.7x^4 - 9375.5x^3 + 3527.7x^2 - 476.08x + 154.66$	$\overline{C}_{44}[c(Cr)]$	$y = 1876.5x^3 - 1373.2x^2 + 309.7x + 92.402$

influence the predicted relaxation volumes derived from the stress method. Here the calculations were performed using the lattice parameter of 2.831 Å, whereas random Fe-Cr alloy structures can adopt the equilibrium lattice parameters up to 2.842 Å. Also, the computed relaxation volumes may differ depending on the elastic constants used in the calculations. As was noted previously, the average elastic constants $\overline{C}_{11}$, $\overline{C}_{12}$, $\overline{C}_{44}$ are the interpolations derived from DFT calculations and hence they may differ from the values computed for each specific structure. Moreover, the elastic constants were computed for the equilibrium lattice parameter whereas they were applied for the prediction of relaxation volumes derived from stresses computed for structures with fixed lattice parameter of 2.831 Å. Furthermore, slightly different convergence parameters were used in the calculations performed using stress and cell relaxation methods. For example, the plane-wave energy cut-off for the fixed-volume calculations was 300 eV whereas for those with full cell relaxation it was 400 eV.

Table A.4
Equations for the trend lines of diagonal (P_{ii} in eV) elements of elastic dipole tensor for vacancies and elements of elastic dipole tensor (P_{11}, $P_{22/33}$, P_{23}, $P_{12/13}$ in eV) for dumbbells as a function of chromium concentration ($c(Cr)$) in random Fe-Cr alloy structures.

Parameter	Variation as a function of the variable in square brackets, denoted here as x	Parameter	Variation as a function of the variable in square brackets, denoted here as x
	Elastic dipole tensors for vacancies (see Fig. 6a and b)		
$P_{11}[c(Cr)]$	$y = \begin{cases} -2.73089x - 4.60421 & \text{for } x \leqslant 0.1 \\ -5.62277x - 4.41065 & \text{for } x > 0.1 \end{cases}$	$P_{22}[c(Cr)]$	$y = \begin{cases} -5.55749x - 4.51942 & \text{for } x \leqslant 0.1 \\ -5.52298x - 4.48534 & \text{for } x > 0.1 \end{cases}$
$P_{33}[c(Cr)]$	$y = \begin{cases} -6.11801x - 4.49765 & \text{for } x \leqslant 0.1 \\ -5.45409x - 4.50325 & \text{for } x > 0.1 \end{cases}$		
	Elastic dipole tensors for dumbbells (see Fig. 7a–d)		
$P_{11}^{Fe\text{-}Fe}[c(Cr)]$	$y = \begin{cases} -21.79723x + 23.60046 & \text{for } x \leqslant 0.1 \\ 3.73925x + 21.41589 & \text{for } x > 0.1 \end{cases}$	$P_{22/33}^{Fe\text{-}Fe}[c(Cr)]$	$y = \begin{cases} -28.79147x + 19.55029 & \text{for } x \leqslant 0.1 \\ 0.91732x + 16.75473 & \text{for } x > 0.1 \end{cases}$
$P_{11}^{Fe\text{-}Cr}[c(Cr)]$	$y = \begin{cases} -0.95036x + 21.64462 & \text{for } x \leqslant 0.1 \\ 2.20376x + 21.49155 & \text{for } x > 0.1 \end{cases}$	$P_{22/33}^{Fe\text{-}Cr}[c(Cr)]$	$y = \begin{cases} -6.79236x + 19.36198 & \text{for } x \leqslant 0.1 \\ -0.85781x + 18.75012 & \text{for } x > 0.1 \end{cases}$
$P_{11}^{Cr\text{-}Cr}[c(Cr)]$	$y = \begin{cases} -11.20776x + 20.84527 & \text{for } x \leqslant 0.1 \\ 3.38226x + 20.05774 & \text{for } x > 0.1 \end{cases}$	$P_{22/33}^{Cr\text{-}Cr}[c(Cr)]$	$y = \begin{cases} -3.24615x + 20.37921 & \text{for } x \leqslant 0.1 \\ 1.13097x + 19.82221 & \text{for } x > 0.1 \end{cases}$
$P_{23}^{Fe\text{-}Fe}[c(Cr)]$	$y = 1.07363x + 4.61543$	$P_{12/13}^{Fe\text{-}Fe}[c(Cr)]$	$y = 1.5062x - 0.38669$
$P_{23}^{Fe\text{-}Cr}[c(Cr)]$	$y = 0.32636x + 4.42626$	$P_{12/13}^{Fe\text{-}Cr}[c(Cr)]$	$y = 0.6145x - 0.15704$
$P_{23}^{Cr\text{-}Cr}[c(Cr)]$	$y = -2.44943x + 3.1727$	$P_{12/13}^{Cr\text{-}Cr}[c(Cr)]$	$y = -0.75586x + 1.34013$

Table A.5
Equations for the trend lines of von Mises stresses (σ_{vM} in MPa) obtained from the invariants of elastic dipole tensors – I_1^P, I_2^P – and first invariant of relaxation volume tensor ($I_1^\Omega = \Omega_{rel}$ in Å^3) computed for vacancies and dumbbells as a function of chromium concentration ($c(Cr)$) in random Fe-Cr alloy structures with a fixed volume equal to 2836.15 Å^3.

Parameter	Variation as a function of the variable in square brackets, denoted here as x	Parameter	Variation as a function of the variable in square brackets, denoted here as x
	σ_{vM} for vacancies (see Fig. 8a)		$I_1^\Omega = \Omega_{rel}$ for vacancies (see Fig. 8c)
$\sigma_{vM}^{vac(Fe)}[c(Cr)]$	$y = \begin{cases} 54.89x + 46.60 & \text{for } x \leqslant 0.1 \\ 86.04x + 36.17 & \text{for } x > 0.1 \end{cases}$	$\Omega_{rel}^{vac(Fe)}[c(Cr)]$	$y = \begin{cases} -15.957x - 3.126 & \text{for } x \leqslant 0.1 \\ -2.175x - 4.593 & \text{for } x > 0.1 \end{cases}$
$\sigma_{vM}^{vac(Cr)}[c(Cr)]$	$y = \begin{cases} 28.97x + 55.32 & \text{for } x \leqslant 0.1 \\ 278.33x + 24.19 & \text{for } x > 0.1 \end{cases}$	$\Omega_{rel}^{vac(Cr)}[c(Cr)]$	$y = \begin{cases} 4.515x - 4.743 & \text{for } x \leqslant 0.1 \\ -4.021x - 3.851 & \text{for } x > 0.1 \end{cases}$
	σ_{vM} for dumbbells (see Fig. 8b)		$I_1^\Omega = \Omega_{rel}$ for dumbbells (see Fig. 8d)
$\sigma_{vM}^{Fe\text{-}Fe}[c(Cr)]$	$y = \begin{cases} 319.76x + 503.18 & \text{for } x \leqslant 0.1 \\ -17.90x + 575.23 & \text{for } x > 0.1 \end{cases}$	$\Omega_{rel}^{Fe\text{-}Fe}[c(Cr)]$	$y = \begin{cases} -12.984x + 17.93 & \text{for } x \leqslant 0.1 \\ -4.776x + 17.192 & \text{for } x > 0.1 \end{cases}$
$\sigma_{vM}^{Fe\text{-}Cr}[c(Cr)]$	$y = \begin{cases} 272.57x + 446.67 & \text{for } x \leqslant 0.1 \\ 60.58x + 481.42 & \text{for } x > 0.1 \end{cases}$	$\Omega_{rel}^{Fe\text{-}Cr}[c(Cr)]$	$y = \begin{cases} 4.171x + 17.408 & \text{for } x \leqslant 0.1 \\ -6.777x + 18.498 & \text{for } x > 0.1 \end{cases}$
$\sigma_{vM}^{Cr\text{-}Cr}[c(Cr)]$	$y = \begin{cases} 288.32x + 477.19 & \text{for } x \leqslant 0.1 \\ -122.73x + 501.15 & \text{for } x > 0.1 \end{cases}$	$\Omega_{rel}^{Cr\text{-}Cr}[c(Cr)]$	$y = \begin{cases} 3.755x + 17.708 & \text{for } x \leqslant 0.1 \\ -5.618x + 18.779 & \text{for } x > 0.1 \end{cases}$

Table A.6
Equations for the trend lines of relaxation volumes (Ω_{rel} in Å^3) for vacancies and dumbbells in random Fe-Cr alloys as a function of the number of Cr atoms in the vicinity of a defect (N_{Cr}^{def}) and as a function of change of magnitudes of magnetic moments (ΔM in μ_B) caused by a defect for the alloy with 5% at. Cr.

Parameter	Variation as a function of the variable in square brackets, denoted here as x	Parameter	Variation as a function of the variable in square brackets, denoted here as x
	Ω_{rel} for vacancies (see Fig. 9a)		
$\Omega_{rel}^{vac(Fe)}[N_{Cr}^{def}]$	$y = \begin{cases} -0.3185x - 3.968 & \text{for } x \leqslant 3 \\ -0.1766x - 4.3859 & \text{for } x \geqslant 3 \end{cases}$	$\Omega_{rel}^{vac(Cr)}[N_{Cr}^{def}]$	$y = \begin{cases} 0.2393x - 4.791 & \text{for } x \leqslant 3 \\ -0.2965x - 3.5152 & \text{for } x \geqslant 3 \end{cases}$
	Ω_{rel} for vacancies in alloy with 5% at. Cr (see Figs. 9c and 12a)		
$\Omega_{rel}^{vac(Fe)}[N_{Cr}^{def}]$	$y = 0.2662x - 4.5148$	$\Omega_{rel}^{vac(Fe)}[\Delta M]$	$y = 0.385x - 3.591$, $R^2 = 0.157$
$\Omega_{rel}^{vac(Cr)}[N_{Cr}^{def}]$	$y = 0.6806x - 5.4627$	$\Omega_{rel}^{vac(Cr)}[\Delta M]$	$y = 0.565x - 4.734$, $R^2 = 0.813$
	Ω_{rel} for dumbbells (see Fig. 9b)		
$\Omega_{rel}^{Fe\text{-}Fe}\left[N_{Cr}^{def}\right]$	$y = \begin{cases} -0.208x + 17.176 & \text{for } x \leqslant 3 \\ -0.018x + 16.486 & \text{for } x \geqslant 3 \end{cases}$	$\Omega_{rel}^{Fe\text{-}Cr}\left[N_{Cr}^{def}\right]$	$y = \begin{cases} 0.006x + 17.424 & \text{for } x \leqslant 3 \\ -0.113x + 17.595 & \text{for } x \geqslant 3 \end{cases}$
$\Omega_{rel}^{Cr\text{-}Cr}\left[N_{Cr}^{def}\right]$	$y = \begin{cases} -0.169x + 18.055 & \text{for } x \leqslant 3 \\ -0.002x + 17.331 & \text{for } x \geqslant 3 \end{cases}$		
	Ω_{rel} for dumbbells in alloy with 5% at. Cr (see Figs. 9d and 12b)		
$\Omega_{rel}^{Fe\text{-}Fe}\left[N_{Cr}^{def}\right]$	$y = -0.3632x + 17.782$	$\Omega_{rel}^{Fe\text{-}Fe(Fe)}[\Delta M]$	$y = 0.858x + 21.519$, $R^2 = 0.293$
		$\Omega_{rel}^{Fe\text{-}Cr(Fe)}[\Delta M]$	$y = 0.599x + 20.767$, $R^2 = 0.396$
$\Omega_{rel}^{Fe\text{-}Cr}\left[N_{Cr}^{def}\right]$	$y = -0.1552x + 18.204$	$\Omega_{rel}^{Fe\text{-}Cr(Cr)}[\Delta M]$	$y = 0.446x + 19.184$, $R^2 = 0.453$
$\Omega_{rel}^{Cr\text{-}Cr}\left[N_{Cr}^{def}\right]$	$y = 0.2287x + 17.265$	$\Omega_{rel}^{Cr\text{-}Cr(Cr)}[\Delta M]$	$y = 0.403x + 19.425$, $R^2 = 0.351$

To evaluate the effect of differences in elastic constants computed using different energy cutoffs and cell relaxation conditions on the relaxation volumes, we performed additional calculations of elastic constants for Fe-5%Cr alloy structures. Ω_{rel} for a Fe-Cr dumbbell computed using the plane-wave energy cut-off 300 eV and the equilibrium lattice parameter was 17.96 Å^3, for the fixed lattice parameter of 2.831 Å and energy cut-off 400 eV it was 17.56 Å^3 whereas for the energy cut-off 400 eV and the equilibrium lattice parameters it was 17.80 Å^3, and for the interpolated average elastic constants it was 17.60 Å^3. Variation of results is of the order of 2%, which shows that the inaccuracy of prediction of elastic constants for alloy structures might be one of the main reasons for the variation in relaxation volumes computed using cell relaxation and stress methods. We note also that the above inaccuracy does not influence significantly the formation energies of point defect since the correction terms computed with different elastic constants do not differ by more than 1 meV.

Finally, we note that the values computed using the fixed cell volume method (the stress method) do not take into account the non-elastic (non-harmonic) effects, which are implicitly included in the results obtained using the cell relaxation method. From the comparison of values of E_{form} obtained using the stress method and the cell relaxation method, shown in Fig. 13d, it is reasonable to expect that the non-harmonic effects would play a particularly significant part in magnetic Fe-Cr alloys with low Cr concentration.

5. Conclusions

Concluding this study, we would like to highlight the clear benefits of an approach combining *ab initio* treatment of defects with auxiliary analysis based on elasticity. This has enabled quantifying the elastic effects of expansion and contraction of the lattice due to the fact that the atoms forming the alloy have different volumes. For example, we found that the volume of a substitutional Cr atom in bcc Fe lattice is approximately 18% larger than the volume of a host Fe atom. At the same time, the volume of a substitutional Fe atom in bcc Cr is 5% smaller than the volume of a host Cr atom. We also found that elastic dipole and relaxation volume tensors of vacancies and SIA defects exhibit large fluctuations, with vacancies showing negative and SIA large positive relaxation volumes. Dipole tensors of vacancies are nearly isotropic across the entire alloy composition range. Fe-Fe and Fe-Cr SIA dumbbells are more anisotropic than Cr-Cr dumbbells. Fluctuations of elastic dipole tensors of SIA defects are primarily associated with the variable orientation of defects. Statistical properties of tensors elastic dipole and relaxation volume tensors are analysed using their principal invariants, showing that properties of point defects differ significantly in alloys containing below and above 10% at. Cr. The von Mises stresses caused by dumbbells in Fe-Cr alloys are

notably larger than those caused by vacancies, which means that the accumulation of dumbbell SIA defects in irradiated materials gives rise to the significantly larger internal stresses, and the resulting deformations, than the accumulation of vacancies. The relaxation volume of a vacancy depends sensitively on whether it occupies a Fe or a Cr lattice site. The observed correlation between the elastic relaxation volumes and magnetic moments of defects suggests that magnetism is a significant factor influencing elastic fields of defects in Fe-Cr alloys. These results also illustrate the significance of elastic relaxation effects in Fe-Cr alloys in the context of treatment of extended defects such as dislocation or grain boundaries, where elastic relaxation may affect segregation and diffusion of solute atoms in the alloy.

CRediT authorship contribution statement

Jan S. Wróbel: Conceptualization, Methodology, Resources, Formal analysis, Data curation, Writing - original draft, Writing - review & editing, Funding acquisition. **Marcin R. Zemła:** Methodology, Formal analysis, Data curation, Visualization, Writing - review & editing. **Duc Nguyen-Manh:** Conceptualization, Methodology, Data curation, Writing - review & editing. **Pär Olsson:** Resources, Writing - review & editing. **Luca Messina:** Resources, Data curation, Writing - review & editing. **Christophe Domain:** Resources, Data curation, Writing - review & editing. **Tomasz Wejrzanowski:** Supervision. **Sergei L. Dudarev:** Conceptualization, Methodology, Writing - original draft, Writing - review & editing, Supervision, Funding acquisition.

Declaration of Competing Interest

The authors declare that they have no known competing financial interests or personal relationships that could have appeared to influence the work reported in this paper.

Acknowledgements

This work has been carried out within the framework of the EUROfusion Consortium and has received funding from the Euratom research and training programme 2014–2018 and 2019–2020 under Grant Agreement No. 633053, and by the M4F project under Grant Agreement No. 755039. The views and opinions expressed herein do not necessarily reflect those of the European Commission. We acknowledge funding by the RCUK Energy Programme (Grant No. EP/T012250/1). The work at WUT has been carried out as a part of an international project co-financed from the funds of the program of the Polish Minister of Science and Higher Education entitled "PMW" in 2019; Agreement No. 5018/H2020-Euratom/2019/2. J.S.W. and D.N.M. acknowledge the support from high-performing computing facility MARCONI (Bologna, Italy) provided by EUROfusion. The simulations were also carried out with the support of the Poznan Supercomputing and Networking Center PCSS under Grant No. 274. For the database of random Fe-Cr alloys, we acknowledge the use of resources on the EDF HPC Athos, Porthos and Gaia supercomputers, representing about 50 million CPU core hours. C. D. acknowledge GENCI resources for some of the calculations (project DeFeT A0050910624). We would like to thank P.-W. Ma, D. R. Mason and M.-C. Marinica for stimulating discussions.

Appendix A

See Tables A.2–A.6 contain equations for the trend lines that were shown in Figures in the main text.

Appendix B. Supplementary data

Supplementary data associated with this article can be found, in the online version, at https://doi.org/10.1016/j.commatsci.2021.110435.

References

[1] W. Cai, W.D. Nix, Imperfections in Crystalline Solids, Cambridge University Press, Cambridge, England, UK, 2016, 10.1017/CBO9781316389508.023.
[2] A.V. Ruban, P.A. Korzhavyi, B. Johansson, First-principles theory of magnetically driven anomalous ordering in bcc Fe-Cr alloys, Phys. Rev. B 77 (9) (2008), 094436, https://doi.org/10.1103/PhysRevB.77.094436.
[3] J.S. Wróbel, D. Nguyen-Manh, M.Y. Lavrentiev, M. Muzyk, S.L. Dudarev, Phase stability of ternary fcc and bcc Fe-Cr-Ni alloys, Phys. Rev. B 91 (2) (2015), 024108, https://doi.org/10.1103/PhysRevB.91.024108.
[4] M.Y. Lavrentiev, R. Drautz, D. Nguyen-Manh, T.P.C. Klaver, S.L. Dudarev, Monte Carlo study of thermodynamic properties and clustering in the bcc Fe-Cr system, Phys. Rev. B 75 (1) (2007), 014208, https://doi.org/10.1103/PhysRevB.75.014208.
[5] J.S. Wróbel, D. Nguyen-Manh, K.J. Kurzydłowski, S.L. Dudarev, A first-principles model for anomalous segregation in dilute ternary tungsten-rhenium-vacancy alloys, J. Phys. Condens. Matter 29 (14) (2017), 145403, https://doi.org/10.1088/1361-648X/aa5f37.
[6] A. Fernandez-Caballero, J.S. Wróbel, P. Mummery, D. Nguyen-Manh, Short-range order in high-entropy alloys: Theoretical formulation and application to Mo-Nb-Ta-V-W system, J. Phase Equilib. Diff. 38 (2017) 391, https://doi.org/10.1007/s11669-017-0582-3.
[7] M. Fedorov, J.S. Wróbel, A. Fernández-Caballero, K.J. Kurzydłowski, D. Nguyen-Manh, Phase stability and magnetic properties in fcc Fe-Cr-Mn-Ni alloys from first-principles modeling, Phys. Rev. B 101 (2020), 174416, https://doi.org/10.1103/PhysRevB.101.174416.
[8] G. Leibfried, N. Breuer, Point Defects in Metals I: Introduction to the Theory, Springer-Verlag, Berlin, Germany, 1978, https://doi.org/10.1007/BFb0045966.
[9] D.J. Bacon, D.M. Barnett, R.O. Scattergood, Anisotropic continuum theory of lattice defects, Prog. Mater. Sci. 23 (1979) 51–262, https://doi.org/10.1016/0079-6425(80)90007-9.
[10] C. Freysoldt, B. Grabowski, T. Hickel, J. Neugebauer, G. Kresse, A. Janotti, C. G. Van de Walle, First-principles calculations for point defects in solids, Rev. Mod. Phys. 86 (1) (2014) 253–305, https://doi.org/10.1103/RevModPhys.86.253.
[11] E. Clouet, S. Garruchet, H. Nguyen, M. Perez, C.S. Becquart, Dislocation interaction with C in α-Fe: A comparison between atomic simulations and elasticity theory, Acta Mater. 56 (2008) 3450–3460, https://doi.org/10.1016/j.actamat.2008.03.024.
[12] C. Varvenne, F. Bruneval, M.-C. Marinica, E. Clouet, Point defect modeling in materials: Coupling *ab initio* and elasticity approaches, Phys. Rev. B 88 (13) (2013), 134102, https://doi.org/10.1103/PhysRevB.88.134102.
[13] C. Varvenne, E. Clouet, Elastic dipoles of point defects from atomistic simulations, Phys. Rev. B 96 (22) (2017), 224103, https://doi.org/10.1103/PhysRevB.96.224103.
[14] S.L. Dudarev, P.-W. Ma, Elastic fields, dipole tensors, and interaction between self-interstitial atom defects in bcc transition metals, Phys. Rev. Mater. 2 (3) (2018), 033602, https://doi.org/10.1103/PhysRevMaterials.2.033602.
[15] P.-W. Ma, S.L. Dudarev, Universality of point defect structure in body-centered cubic metals, Phys. Rev. Mater. 3 (1) (2019), 013605, https://doi.org/10.1103/PhysRevMaterials.3.013605.
[16] P.-W. Ma, S.L. Dudarev, Effect of stress on vacancy formation and migration in body-centered-cubic metals, Phys. Rev. Mater. 3 (6) (2019), 063601, https://doi.org/10.1103/PhysRevMaterials.3.063601.
[17] P.-W. Ma, S.L. Dudarev, Symmetry-broken self-interstitial defects in chromium, molybdenum, and tungsten, Phys. Rev. Mater. 3 (4) (2019), 043606, https://doi.org/10.1103/PhysRevMaterials.3.043606.
[18] C. Domain, C.S. Becquart, *Ab initio* calculations of defects in Fe and dilute Fe-Cu alloys, Phys. Rev. B 65 (2) (2001), 024103, https://doi.org/10.1103/PhysRevB.65.024103.
[19] S.L. Dudarev, M.R. Gilbert, K. Arakawa, H. Mori, Z. Yao, M.L. Jenkins, P.M. Derlet, Langevin model for real-time Brownian dynamics of interacting nanodefects in irradiated metals, Phys. Rev. B 81 (22) (2010), 224107, https://doi.org/10.1103/PhysRevB.81.224107.
[20] S.L. Dudarev, D.R. Mason, E. Tarleton, P.-W. Ma, A.E. Sand, A multi-scale model for stresses, strains and swelling of reactor components under irradiation, Nucl. Fusion 58 (12) (2018), 126002, https://doi.org/10.1088/1741-4326/aadb48.
[21] E. Clouet, C. Varvenne, T. Jourdan, Elastic modeling of point-defects and their interaction, Comput. Mater. Sci. 147 (2018) 49–63, https://doi.org/10.1016/j.commatsci.2018.01.053.
[22] J.S. Wróbel, D. Nguyen-Manh, S.L. Dudarev, K.J. Kurzydłowski, Point defect properties of ternary fcc Fe-Cr-Ni alloys, Nucl. Instr. Meth. Phys. Res. B 393 (2017) 126–129, https://doi.org/10.1016/j.nimb.2016.10.024.
[23] A.J. Samin, D.A. Andersson, E.F. Holby, B.P. Uberuaga, *Ab initio* based examination of the kinetics and thermodynamics of oxygen in Fe-Cr alloys, Phys. Rev. B 99 (17) (2019), 174202, https://doi.org/10.1103/PhysRevB.99.174202.
[24] D. Costa, G. Adjanor, C.S. Becquart, P. Olsson, C. Domain, Vacancy migration energy dependence on local chemical environment in Fe-Cr alloys: A Density Functional Theory study, J. Nucl. Mater. 452 (1–3) (2014) 425–433, https://doi.org/10.1016/j.jnucmat.2014.05.007.
[25] T.P.C. Klaver, R. Drautz, M.W. Finnis, Magnetism and thermodynamics of defect-free Fe-Cr alloys, Phys. Rev. B 74 (9) (2006), 094435, https://doi.org/10.1103/PhysRevB.74.094435.
[26] T.P.C. Klaver, P. Olsson, M.W. Finnis, Interstitials in FeCr alloys studied by density functional theory, Phys. Rev. B 76 (21) (2007), 214110, https://doi.org/10.1103/PhysRevB.76.214110.

[27] M.Y. Lavrentiev, S.L. Dudarev, D. Nguyen-Manh, Magnetic cluster expansion simulations of FeCr alloys, J. Nucl. Mater. 386–388 (2009) 22–25, https://doi.org/10.1016/j.jnucmat.2008.12.052.

[28] M.Y. Lavrentiev, D. Nguyen Manh, S.L. Dudarev, Magnetic cluster expansion study of chromium precipitates in Fe-Cr alloys, Solid State Phenom. 172–174 (2011) 1002–1007, https://doi.org/10.4028/www.scientific.net/SSP.172-174.1002.

[29] D. Nguyen-Manh, M.Y. Lavrentiev, S.L. Dudarev, Magnetic origin of nano-clustering and point defect interaction in Fe-Cr alloys: an ab initio study, J. Comput.-Aided Mater. Des. 14 (S1) (2007) 159–169. doi:10.1007/s10820-007-9079-4.

[30] D. Nguyen-Manh, M.Y. Lavrentiev, S.L. Dudarev, The Fe-Cr system: atomistic modelling of thermodynamics and kinetics of phase transformations, C.R. Phys. 9 (3–4) (2008) 379–388, https://doi.org/10.1016/j.crhy.2007.10.011.

[31] D. Nguyen-Manh, M.Y. Lavrentiev, M. Muzyk, S.L. Dudarev, First-principles models for phase stability and radiation defects in structural materials for future fusion power-plant applications, J. Mater. Sci. 47 (21) (2012) 7385–7398, https://doi.org/10.1007/s10853-012-6657-y.

[32] P. Olsson, I.A. Abrikosov, L. Vitos, J. Wallenius, *Ab initio* formation energies of Fe-Cr alloys, J. Nucl. Mater. 321 (2003) 84–90, https://doi.org/10.1016/S0022-3115(03)00207-1.

[33] P. Olsson, I.A. Abrikosov, J. Wallenius, Electronic origin of the anomalous stability of Fe-rich bcc Fe-Cr alloys, Phys. Rev. B 73 (10) (2006), 104416, https://doi.org/10.1103/PhysRevB.73.104416.

[34] P. Olsson, C. Domain, J. Wallenius, *Ab initio* study of Cr interactions with point defects in bcc Fe, Phys. Rev. B 75 (1) (2007), 014110, https://doi.org/10.1103/PhysRevB.75.014110.

[35] O. Senninger, F. Soisson, E. Martínez, M. Nastar, C.-C. Fu, Y. Bréchet, Modeling radiation induced segregation in iron-chromium alloys, Acta Mater. 103 (2016) 1–11, https://doi.org/10.1016/j.actamat.2015.09.058.

[36] I. Mirebeau, G. Parette, Neutron study of the short range order inversion in $Fe_{1-x}Cr_x$, Phys. Rev. B 82 (10) (2010), 104203, https://doi.org/10.1103/PhysRevB.82.104203.

[37] C.D. Hardie, C.A. Williams, S. Xu, S.G. Roberts, Effects of irradiation temperature and dose rate on the mechanical properties of self-ion implanted Fe and Fe-Cr alloys, J. Nucl. Mater. 439 (1–3) (2013) 33–40, https://doi.org/10.1016/j.jnucmat.2013.03.052.

[38] S. Porollo, A. Dvoriashin, A. Vorobyev, Y. Konobeev, The microstructure and tensile properties of Fe-Cr alloys after neutron irradiation at 400°C to 5.5-7.1 dpa, J. Nucl. Mater. 256 (2–3) (1998) 247–253, https://doi.org/10.1016/S0022-3115(98)00043-9.

[39] V. Kuksenko, C. Pareige, C. Genevois, F. Cuvilly, M. Roussel, P. Pareige, Effect of neutron-irradiation on the microstructure of a Fe-12at.%Cr alloy, J. Nucl. Mater. 415 (1) (2011) 61–66, https://doi.org/10.1016/j.jnucmat.2011.05.042.

[40] M.Y. Lavrentiev, D. Nguyen-Manh, S.L. Dudarev, Chromium-vacancy clusters in dilute bcc Fe-Cr alloys: An *ab initio* study, J. Nucl. Mater. 499 (2018) 613–621, https://doi.org/10.1016/j.jnucmat.2017.10.038.

[41] T.P.C. Klaver, E. del Rio, G. Bonny, S.M. Eich, A. Caro, Inconsistencies in modelling interstitials in FeCr with empirical potentials, Comput. Mater. Sci. 121 (2016) 204–208, https://doi.org/10.1016/j.commatsci.2016.04.033.

[42] C.S. Becquart, R. Ngayam Happy, P. Olsson, C. Domain, A DFT study of the stability of SIAs and small SIA clusters in the vicinity of solute atoms in Fe, J. Nucl. Mater. 500 (2018) 92–109, https://doi.org/10.1016/j.jnucmat.2017.12.022.

[43] F. Hofmann, D. Nguyen-Manh, M.R. Gilbert, C.E. Beck, J.K. Eliason, A.A. Maznev, W. Liu, D.E.J. Armstrong, K.A. Nelson, S.L. Dudarev, Lattice swelling and modulus change in a helium-implanted tungsten alloy: X-ray micro-diffraction, surface acoustic wave measurements, and multiscale modelling, Acta Mater. 89 (2015) 352–363, https://doi.org/10.1016/j.actamat.2015.01.055.

[44] D.R. Mason, D. Nguyen-Manh, M.-C. Marinica, R. Alexander, A.E. Sand, S.L. Dudarev, Relaxation of microscopic and mesoscopic irradiation-induced defects in tungsten, J. Appl. Phys. 126 (2019) 075112. doi:10.1063.1.5098452.

[45] P.-W. Ma, S.L. Dudarev, CALANIE: Anisotropic elastic correction to the total energy, to mitigate the effect of periodic boundary conditions, Comput. Phys. Commun. 252 (2019), 107130, https://doi.org/10.1016/j.cpc.2019.107130.

[46] T. Mura, Micromechanics of Defects in Solids, 2nd Edition,, Kluwer Academic Publishers, Dordrecht, 1987, 10.1007/978-94-009-3489-4.

[47] P.T. Heald, M.V. Speight, Point defect behaviour in irradiated materials, Acta Metall. 23 (1975) 1389–1399, https://doi.org/10.1016/0001-6160(75)90148-0.

[48] K. Naumenko, H. Altenbach, Modeling of Creep for Structural Analysis, Springer Science & Business Media, 2007.

[49] J.F. Nye, Physical Properties of Crystals, Oxford Science Publications, Clarendon Press, Oxford, 1985, https://doi.org/10.1002/crat.2170211204.

[50] L.D. Landau, E.M. Lifshitz, Statistical Physics, second ed., Pergamon Press, Oxford, England, 1969, 10.1016/C2009-0-24487-4.

[51] J.B. Piochaud, T.P.C. Klaver, G. Adjanor, P. Olsson, C. Domain, C.S. Becquart, First-principles study of point defects in an fcc Fe-10Ni-20Cr model alloy, Phys. Rev. B 89 (2) (2014), 024101, https://doi.org/10.1103/PhysRevB.89.024101.

[52] G. Kresse, D. Joubert, From ultrasoft pseudopotentials to the projector augmented-wave method, Phys. Rev. B 59 (1999) 1758–1775, https://doi.org/10.1103/PhysRevB.59.1758.

[53] P.E. Blöchl, Projector augmented-wave method, Phys. Rev. B 50 (1994) 17953–17979, https://doi.org/10.1103/PhysRevB.50.17953.

[54] G. Kresse, J. Furthmüller, Efficient iterative schemes for *ab initio* total-energy calculations using a plane-wave basis set, Phys. Rev. B 54 (1996) 11169–11186, https://doi.org/10.1103/PhysRevB.54.11169.

[55] G. Kresse, J. Furthmüller, Efficiency of *ab initio* total energy calculations for metals and semiconductors using a plane-wave basis set, Comput. Mater. Sci. 6 (1) (1996) 15–50, https://doi.org/10.1016/0927-0256(96)00008-0.

[56] J.P. Perdew, K. Burke, M. Ernzerhof, Generalized gradient approximation made simple, Phys. Rev. Lett. 77 (1996) 3865–3868, https://doi.org/10.1103/PhysRevLett.77.3865.

[57] D. Nguyen-Manh, P.-W. Ma, M.Y. Lavrentiev, S.L. Dudarev, Constrained non-collinear magnetism in disordered Fe and Fe-Cr alloys, Ann. Nucl. Energy 77 (2015) 246–251, https://doi.org/10.1016/j.annucene.2014.10.042.

[58] H.J. Monkhorst, J.D. Pack, Special points for Brillouin zone integrations, Phys. Rev. B 13 (1976) 5188–5192, https://doi.org/10.1103/PhysRevB.13.5188.

[59] N. Castin, L. Messina, C. Domain, R.C. Pasianot, P. Olsson, Improved atomistic Monte Carlo models based on *ab initio*-trained neural networks: Application to FeCu and FeCr alloys, Phys. Rev. B 95 (21) (2017), 214117, https://doi.org/10.1103/PhysRevB.95.214117.

[60] N. Castin, M.I. Pascuet, L. Messina, C. Domain, P. Olsson, R.C. Pasianot, L. Malerba, Advanced atomistic models for radiation damage in Fe-based alloys: contributions and future perspectives from artificial neural networks, Comput. Mater. Sci. 148 (2018) 116–130, https://doi.org/10.1016/j.commatsci.2018.02.025.

[61] R. Hultgren, P.D. Desai, D.T. Hawkins, M. Gleiser, K.K. Kelley, Selected Values of the Thermodynamic Properties of Binary Alloys, American Society for Metals, Metals Park, Ohio, 1973.

[62] W.P. Pearson, A Handbook of Lattice Spacings and Structures of Metals and Alloys, Pergamon Press, London, 1958.

[63] S.L. Dudarev, Density functional theory models for radiation damage, Annu. Rev. Mater. Res. 43 (1) (2013) 35–61, https://doi.org/10.1146/annurev-matsci-071312-121626.

[64] F. Willaime, C.-C. Fu, M.-C. Marinica, J. Dalla Torre, Stability and mobility of self-interstitials and small interstitial clusters in α-iron: *Ab initio* and empirical potential calculations, Nucl. Instr. Meth. Phys. Res. B 228 (1–4 SPEC. ISS.) (2005) 92–99. doi:10.1016/j.nimb.2004.10.028.

[65] P. Olsson, *Ab initio* study of interstitial migration in Fe-Cr alloys, J. Nucl. Mater. 386–388 (2009) 86–89, https://doi.org/10.1016/j.jnucmat.2008.12.065.

[66] L. Messina, T. Schuler, M. Nastar, M.-C. Marinica, P. Olsson, Solute diffusion by self-interstitial defects and radiation-induced segregation in ferritic Fe-X (X=Cr, Cu, Mn, Ni, P, Si) dilute alloys, Acta Mater. 191 (2020) 166–185, https://doi.org/10.1016/j.actamat.2020.03.038.

[67] V.I. Razumovskiy, A.V. Ruban, P.A. Korzhavyi, First-principles study of elastic properties of Cr- and Fe-rich Fe-Cr alloys, Phys. Rev. B 84 (2) (2011), 024106, https://doi.org/10.1103/PhysRevB.84.024106.

[68] H. Zhang, B. Johansson, L. Vitos, *Ab initio* calculations of elastic properties of bcc Fe-Mg and Fe-Cr random alloys, Phys. Rev. B 79 (22) (2009), 224201, https://doi.org/10.1103/PhysRevB.79.224201.

[69] G.D. Preston B.A., XXXV. An X-ray examination of iron-chromium alloys, London, Edinburgh Dublin Philos. Mag. J. Sci. 13 (84) (1932) 419–425, https://doi.org/10.1080/14786443209461944.

[70] A.L. Sutton, W. Hume-Rothery, CXLI. The lattice spacings of solid solutions of titanium, vanadium, chromium, manganese, cobalt and nickel in α-iron, London, Edinburgh Dublin Philos. Mag. J. Sci. 46 (383) (1955) 1295–1309, https://doi.org/10.1080/14786441208521140.

[71] G.R. Speich, A.J. Schwoeble, W.C. Leslie, Elastic constants of binary iron-base alloys, Metall. Trans. 3 (8) (1972) 2031–2037, https://doi.org/10.1007/BF02643211.

[72] J.A. Rayne, B.S. Chandrasekhar, Elastic Constants of Iron from 4.2 to 300 K, Phys. Rev. 122 (1961) 1714–1716, https://doi.org/10.1103/PhysRev.122.1714.

[73] D. Dever, Temperature dependence of the elastic constants in α-iron single crystals: relationship to spin order and diffusion anomalies, J. Appl. Phys. 43 (8) (1972) 3293–3301, https://doi.org/10.1063/1.1661710.

[74] G. Ghosh, G. Olson, The isotropic shear modulus of multicomponent Fe-base solid solutions, Acta Mater. 50 (10) (2002) 2655–2675, https://doi.org/10.1016/S1359-6454(02)00096-4.

[75] P.M. Derlet, S.L. Dudarev, Microscopic structure of a heavily irradiated material, Phys. Rev. Mater. 4 (2020), 023605, https://doi.org/10.1103/PhysRevMaterials.4.023605.

[76] N.N. Greenwood, A. Earnshaw, Chemistry of the Elements, second ed., Butterworth-Heinemann, Oxford, 1997, 10.1016/C2009-0-30414-6.

[77] Z. Jiao, G.S. Was, Segregation behavior in proton- and heavy-ion-irradiated ferritic-martensitic alloys, Acta Mater. 59 (11) (2011) 4467–4481, https://doi.org/10.1016/j.actamat.2011.03.070.

[78] C. Domain, C.S. Becquart, Solute ⟨111⟩ interstitial loop interaction in α-Fe: A DFT study, J. Nucl. Mater. 499 (2018) 582–594, https://doi.org/10.1016/j.jnucmat.2017.10.070.

[79] C.-C. Fu, F. Willaime, P. Ordejón, Stability and Mobility of Mono- and Di-Interstitials in α-Fe, Phys. Rev. Lett. 92 (2004), 175503, https://doi.org/10.1103/PhysRevLett.92.175503.

[80] D. Nguyen-Manh, A.P. Horsfield, S.L. Dudarev, Self-interstitial atom defects in bcc transition metals: Group-specific trends, Phys. Rev. B 73 (2006), 020101, https://doi.org/10.1103/PhysRevB.73.020101.